HHS Public Access

Author manuscript

Neuron. Author manuscript; available in PMC 2022 April 21.

Published in final edited form as:

Neuron. 2021 April 21; 109(8): 1314–1332.e5. doi:10.1016/j.neuron.2021.02.023.

Presynaptic store-operated Ca^{2+} entry drives excitatory spontaneous neurotransmission and augments endoplasmic reticulum stress

Natali L. Chanaday[1], **Elena Nosyreva**[2], **Ok-Ho Shin**[1], **Hua Zhang**[3], **Iltan Aklan**[4], **Deniz Atasoy**[4,5,6], **Ilya Bezprozvanny**[3,7], **Ege T. Kavalali**[1,8,†]

[1]Department of Pharmacology, School of Medicine, Vanderbilt University, Nashville, TN, 37240-7933, USA.

[2]Department of Neuroscience, The University of Texas Southwestern Medical Center, Dallas, TX 75390-9111, USA.

[3]Department of Physiology, The University of Texas Southwestern Medical Center, Dallas, TX 75390-9040, USA.

[4]Department of Neuroscience and Pharmacology, Carver College of Medicine, University of Iowa, Iowa City, IA, 52242, USA

[5]Iowa Neuroscience Institute, University of Iowa, Iowa City, IA, 52242, USA

[6]FOE Diabetes Research Center, University of Iowa, Iowa City, IA, 52242, USA

[7]Laboratory of Molecular Neurodegeneration, Peter the Great St Petersburg State Polytechnic University, St. Petersburg, Russia.

[8]Vanderbilt Brain Institute.

Summary

Store operated calcium entry (SOCE) is activated by depletion of Ca^{2+} from the endoplasmic reticulum (ER) and mediated by stromal interaction molecule (STIM) proteins. Here, we show that in rat and mouse hippocampal neurons acute ER Ca^{2+} depletion increases presynaptic Ca^{2+} levels and glutamate release through a STIM2 and synaptic Ca^{2+} sensor synaptotagmin-7 (syt7) dependent pathway. In contrast, synaptotagmin-1 (syt1) can suppress SOCE-mediated spontaneous release and STIM2 is required for the increase in spontaneous release seen during syt1 loss-of-

[†]Corresponding author: Ege T. Kavalali, Ph.D., Department of Pharmacology, Vanderbilt University, 465 21st Avenue South, 7130A MRBIII, PMB407933 Nashville, TN 37240-7933, phone: 615-343-5480, ege.kavalali@vanderbilt.edu.

Author contribution

Conceptualization: NLC, EN, IB and ETK. Methodology: NLC, EN, OHS and IA. Software: NLC. Validation, investigation and formal analysis: NLC and EN. Resources: NLC, EN and HZ. Data curation and visualization: NLC. Writing – Original draft: NLC and ETK. Writing – Review and editing: NLC, EN, OHS, HZ, DA, IB and ETK. Supervision: NLC, IB and ETK. Funding acquisition: ETK, IB and NLC.

Declaration of interest

The authors declare no competing interests.

function. We also demonstrate that chronic ER stress activates the same pathway leading to syt7-dependent potentiation of spontaneous glutamate release. During ER stress, inhibition of SOCE or syt7-driven fusion partially restored basal neurotransmission and decreased expression of pro-apoptotic markers indicating that these processes participate in the amplification of ER stress-related damage. Taken together, we propose that presynaptic SOCE links ER stress and augmented spontaneous neurotransmission which may, in turn, facilitate neurodegeneration.

Graphical Abstract

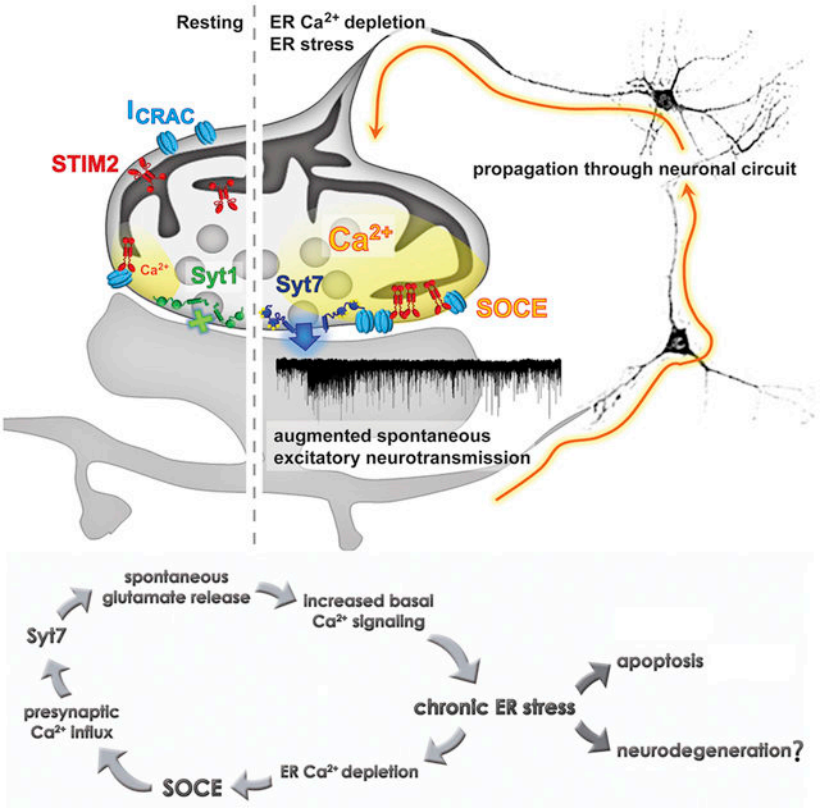

In Brief

Chanaday et al. uncover the underlying molecular mechanism coupling store-operated Ca^{2+} entry to neurotransmitter release at excitatory presynaptic terminals. Activation of this mechanism during chronic ER stress may exacerbate and help propagate the neuronal damage via increased glutamate release.

Introduction

In neurons the endoplasmic reticulum (ER) spans the whole cell volume, including dendritic and axonal processes (Luarte et al., 2018; Wu et al., 2017). While the role of ER and Golgi outposts in dendrite formation, maturation and plasticity has been widely studied (Horton and Ehlers, 2004), the involvement of presynaptic ER in neurotransmission remains unclear (Bezprozvanny and Kavalali, 2020). Recent 3D reconstructions of axons visualized by

scanning electron microscopy revealed that tubular shaped ER is present in the axon and branches into presynaptic boutons, creating a net that surrounds mitochondria, endosomal organelles and synaptic vesicles (Wu et al., 2017). Contact sites of ER with the plasma membrane (PM) were also present in axons (called ER-PM junctions) (Wu et al., 2017).

Store operated Ca^{2+} entry (SOCE) is a process activated by either reduction or depletion of Ca^{2+} in the lumen of the ER, which in turn triggers Ca^{2+} influx into the cytosol followed by replenishment of the ER by the sarco-endoplasmic reticulum Ca^{2+}-ATPase (SERCA) (Prakriya and Lewis, 2015; Putney, 2009; Soboloff et al., 2012). The SOCE response is mediated by the clustering and interaction at ER-PM junctions of the ER Ca^{2+} sensor STIM and the PM Ca^{2+} channel Orai (also known as Ca^{2+} release-activated Ca^{2+} channel or CRAC) (Prakriya and Lewis, 2015; Putney, 2009; Soboloff et al., 2012). Isoforms 1 and 2 of STIM protein (STIM1 and 2) as well as Orai isoforms 1, 2 and 3 are expressed in neurons in the central nervous system where they have been implicated in Ca^{2+} homeostasis (Gruszczynska-Biegala et al., 2011; Klejman et al., 2009; Moccia et al., 2015; Wei et al., 2017). While STIM1 has been shown to mediate classical SOCE response upon ER Ca^{2+} depletion, STIM2, due to its lower Ca**2+** affinity, can respond to subtler decreases in Ca^{2+} concentration and finely tune resting Ca^{2+} levels in neurons (Gruszczynska-Biegala and Kuznicki, 2013; Gruszczynska-Biegala et al., 2011). In fact, STIM2 is the more abundant STIM isoform in hippocampal and cortical neurons (Berna-Erro et al., 2009; Moccia et al., 2015) and its activity has been implicated in the generation, stabilization and maturation of functional dendritic spines through a pathway involving Ca^{2+}-calmodulin kinase II (CaMKII) and microtubules (Korkotian et al., 2017; Pchitskaya et al., 2017; Sun et al., 2014). In contrast, the existence and putative role of SOCE presynaptically remains largely unexplored (Bezprozvanny and Kavalali, 2020; Kavalali, 2019).

Here, we show that SOCE is mediated by STIM2 in hippocampal presynaptic terminals. SOCE activation enhances spontaneous neurotransmission, specifically at excitatory synapses. This increase in spontaneous synaptic vesicle fusion is driven by the Ca^{2+} sensor synaptotagmin-7 (syt7). Conversely, synaptotagmin-1 (syt1) clamps spontaneous fusion driven by basal Ca^{2+} fluctuations elicited by SOCE at rest. Blockade of SOCE or deletion of syt7 partially prevents the neuronal dysregulations caused by chronic ER stress including the increase in presynaptic Ca^{2+} levels, the exacerbated spontaneous glutamate release and the upregulation of apoptotic markers. Our findings elucidate a heretofore overlooked presynaptic pathway that may contribute to the progression of neurodegenerative processes associated with ER stress. These results suggest that SOCE mediated spontaneous release and its impact on ER stress may form a putative therapeutic target for treatment of neurodegenerative diseases.

Results

Activation of presynaptic SOCE triggers spontaneous neurotransmitter release at excitatory synapses

The mechanisms and the role of unconventional Ca^{2+} signaling pathways in regulation of neurotransmitter release, independently of voltage-gated Ca^{2+} channels, remain largely unclear (Kavalali, 2019). SOCE, in particular, has been implicated in axonal growth,

maturation of dendritic spines and postsynaptic plasticity responses (potentiation as well as depression) (Baba et al., 2003; Korkotian et al., 2017; Mitchell et al., 2012; Pchitskaya et al., 2017; Shim et al., 2013; Sun et al., 2014; Zhang et al., 2015), but whether Ca^{2+} influx through SOCE can impact synaptic vesicle release itself remains unknown. To trigger SOCE in hippocampal neurons we used a modified version of the classical Ca^{2+} re-addition method (Bird et al., 2018) and thapsigargin (TG), a blocker of the SERCA, which leads to depletion of ER Ca^{2+} and activation of SOCE. We continuously recorded miniature excitatory postsynaptic currents (mEPSCs) in hippocampal neurons while sequentially perfusing extracellular solutions containing: 2 mM Ca^{2+} (2 min, baseline spontaneous activity), 0 mM Ca^{2+} (1 min, to record Ca^{2+} influx-independent spontaneous neurotransmission) and 2 mM Ca^{2+} with 1 μM TG (Ca^{2+} re-addition for 10 min to simultaneously induce ER Ca^{2+} reduction and SOCE activation; Figure 1A). This protocol caused a moderate but consistent reduction in the levels of ER luminal Ca^{2+}, compared to the more typical strong depletion classically obtained in the absence of extracellular Ca^{2+} (Figure S1A-B) thus allowing us to study the impact of moderate — likely more physiological — changes in ER Ca^{2+} content.

As previously reported, mEPSC frequency was reduced ~50% in the absence of extracellular Ca^{2+} compared to baseline (Figure 1A-F). The subsequent TG perfusion led to a transient and robust increase in the frequency of mEPSCs, with variable intensity and duration among neurons (Figure 1A-F). On average, mEPSC frequency was increased 1.5 to 2-fold after TG treatment (Figure 1E-F), and it was observed in >95% of the pyramidal neurons in dissociated cultures (Figure 1D). When we tested the same protocol on Schaffer collateral synapses onto CA1 pyramidal neurons in acute hippocampal slices we detected a 1.5 to 5.3-fold increase in mEPSC frequency (Figure S1C-D) in agreement with earlier findings (Emptage et al., 2001). Evoked probability of release, on the other hand, was unaffected by this acute partial depletion of ER Ca^{2+}, since amplitudes and paired-pulse ratios of excitatory postsynaptic currents (EPSCs) were not impacted by perfusion of TG (Figure S1E-F). Moreover, the same acute ER Ca^{2+} depletion protocol failed to trigger significant inhibitory spontaneous neurotransmission (Figure S1G-J). Taken together, these results indicate that our experimental protocol causes a partial reduction of intraluminal ER Ca^{2+} levels, which in turn triggers spontaneous release of neurotransmitters at excitatory synapses.

The molecular machinery involved in SOCE responses has been previously shown to be present in neurons (Gruszczynska-Biegala et al., 2011). Isoform 2 of STIM (STIM2) is more abundant in hippocampal neurons than STIM1 (Berna-Erro et al., 2009; Moccia et al., 2015). In our hippocampal cultures, STIM2 had a distribution compatible with the neuronal smooth ER, with positive staining in the cell body, the neurites (both axons and dendrites), presynaptic boutons and dendritic spines (Figure 2A-G). An average of ~60% of presynaptic terminals contained STIM2 (Figure 2C), and ~40% of the total STIM2 positive volume in neurons was localized to axons (Figure 2D) STIM2 was also present in postsynaptic dendrites and spines (Figure 2E-G). These post-synaptic STIM2 levels are consistent with previous reports of 10-50 % of dendritic spines containing smooth ER (Padamsey et al., 2019). Antibody specificity was corroborated by performing STIM2 immunofluorescence staining in cultured hippocampal neurons lacking STIM2 protein (negative control; Figure S2). Further analysis revealed an enrichment of STIM2 in VGluT1-positive presynaptic

boutons in comparison to VGAT-positive ones (Figure 2H-I), with almost half of excitatory presynaptic terminals containing STIM2 versus ~15% in the GABAergic counterparts (Figure 2H-I). This difference can explain the observed selective regulation of mEPSCs by partial ER Ca^{2+} depletion. Super-resolution microscopy (2D-STED) was used to gain more insight into STIM2 subcellular localization in presynaptic terminals (Figure 2J-M). Small clusters of STIM2 were detected in synapsin-1 positive boutons, at both basal (unstimulated, Figure 2J) and TG treated (5 min, Figure 2K) conditions. Some clusters were localized in the opposite region of the bouton with respect to the active zone marker Bassoon, but others were localized at the edges of the Bassoon “active zone” staining (Figure 2J-M), with a mean distance of ~250 nm (Figure 2M). The number of STIM2 clusters per bouton showed a modest increase after ER Ca^{2+} depletion (Figure 2L). Although ER-plasma membrane junctions were previously proposed to be localized away from the active zone (Wu et al., 2017), ER in axon terminals is likely to be mobile, especially after changes in ER Ca^{2+} levels, which may explain our results. Commercially available STIM2 antibodies were not suitable for immunoelectron microscopy in our hands, so we could not explore this notion further. Taken together, the data presented here show that hippocampal neurons robustly express STIM2, indicating that the SOCE machinery is present in synapses, both pre- and postsynaptically.

To assess if a SOCE response underlies the increase in mEPSC frequency observed during acute TG treatment, we repeated the same experimental protocol in neurons lacking STIM2 (STIM2 conditional knock out – cKO –; Figure 3A). Dissociated cultures were prepared from STIM2 conditional (“floxed”) mice and infected with lentivirus containing the Cre recombinase leading to depletion of STIM2 protein after 2 weeks of infection (protein depletion in each experiment was corroborated by GFP expression, also see Figure S2). Basal excitatory neurotransmission was not altered in this setting (Figure 3C). When Ca^{2+} levels in the ER were reduced via TG perfusion there was no change in the frequency of mEPSCs in STIM2 cKO hippocampal neurons (Figure 3B-D), indicating that STIM2 is necessary for the augmentation of spontaneous excitatory neurotransmission. There was also a small increase in mEPSC amplitude in STIM2 cKO neurons compared to controls, indicating an additional role of STIM2 in postsynaptic receptor signaling (see Discussion). The absence of a TG effect in STIM2 cKO neurons was further supported by directly monitoring spontaneous fusion of synaptic vesicles using the vesicular glutamate transporter-1 fused to the pH sensitive GFP (VGluT1-pHluorin; Figure S3) as a probe. While TG led to an increase in the frequency of spontaneous fusion of synaptic vesicles compared to untreated control neurons, it had no effect on STIM2 cKO neurons (Figure S3) indicating that STIM2 participates in the mechanism underlying the TG-mediated increase in mEPSCs within presynaptic terminals. In agreement with this premise, using rat hippocampal neurons and a set of specific shRNAs targeting STIM2 (see methods; Figure S4A-C), we found that ~91% reduction in STIM2 protein completely abolished the augmentation of excitatory spontaneous neurotransmission due to ER Ca^{2+} depletion (Figure S4G and J). This phenotype was rescued by expressing a shRNA-resistant STIM2 (human-STIM2-YFP, Figure S4A-C, G and J). Perfusing TG to deplete Ca^{2+} from the ER still led to an increase in mEPSC frequency, similar to controls, in neurons expressing a knock down (KD) construct for STIM1, the other STIM isoform present in these cells (~88% reduction in protein levels,

Figure S4D-F, H and J). Interestingly, basal mEPSC frequency and amplitude were reduced in STIM1 KD neurons (Figure S4I and K), suggesting that while STIM2 modulates excitatory spontaneous neurotransmission in response to ER Ca^{2+}changes, STIM1 may participate in setting the basal properties of this form of neurotransmission. These changes in STIM1 KD neurons were rescued by expressing a shRNA-resistant STIM1 (human-STIM1-YFP), validating the specificity of the target.

We next examined if the transient decrease in ER Ca^{2+} concentration was impacting presynaptic Ca^{2+} levels. We used the Ca^{2+} indicator GCaMP6s fused to the synaptic vesicle protein synaptobrevin-2 (Syb2) to specifically measure changes in presynaptic Ca^{2+} concentration (Figure 3D). Partial depletion of ER Ca^{2+} led to an increase in presynaptic Ca^{2+} quantified as a rise in GCaMP6s fluorescence slope as well as an increase in the total fluorescence area, compared to untreated control neurons (Figure 3E-G). This increase in presynaptic Ca^{2+} was completely abolished in STIM2 cKO hippocampal neurons, indicating that it is a consequence of SOCE activation. In agreement with our electrophysiological and Ca^{2+} imaging results, it was previously reported that STIM2 mediates Ca^{2+} influx via SOCE in cortical neurons, whereas STIM1 does not participate (Berna-Erro et al., 2009). Using syb2-GCaMP6s, we also observed presynaptic Ca^{2+} sparks (Ross, 2012) but their amplitude and frequency were not affected by TG or STIM2 cKO (data not shown), indicating that basal presynaptic Ca^{2+} levels but not Ca^{2+} transients are involved in SOCE-mediated augmentation of spontaneous neurotransmitter release. To further test if this is a SOCE-dependent mechanism, we pharmacologically inhibited SOCE using the general blocker SKF 96365 (30 μM) and the more CRAC-specific blocker BTP2 (or YM 58483, at 300 nM; Figure 3H-I). Both pharmacological treatments prevented the increase in mEPSC frequency produced by ER Ca^{2+} depletion, with no changes in mEPSC amplitudes (Figure 3H-J). Taken together, our results strongly support that small changes in ER Ca^{2+} levels can trigger SOCE in presynaptic terminals leading to increased presynaptic Ca^{2+} levels and enhancing spontaneous glutamate release at excitatory synapses.

SOCE triggers excitatory spontaneous release through Ca^{2+} binding to synaptotagmin-7

In contrast to action potential evoked neurotransmission, spontaneous fusion of synaptic vesicles is not exclusively dependent on Ca^{2+}, although its rate is modulated by Ca^{2+} fluctuations. The molecular identity of the Ca^{2+} sensor for spontaneous release has been a matter of debate, although it is clear that synaptotagmin-1 (syt1) prevents spontaneous fusion by clamping the fusion machinery in a Ca^{2+}-dependent manner (Chanaday and Kavalali, 2018b; Sudhof, 2013). Reducing syt1 levels (~90% reduction, Figure S5A-C) using a previously validated specific shRNA (syt1 knock down – KD –; see Key Resources Table) unclamped spontaneous release leading to a significant increase in mEPSC frequency (Figure 4A-B). Provoking ER Ca^{2+} depletion by TG perfusion could still reliably trigger spontaneous release in syt1 KD neurons, although the increase was partially occluded by the augmentation in baseline mEPSC frequency (Figure 4A-B). Another member of the synaptotagmin family, synaptotagmin-7 (syt7) is also abundant in hippocampal neurons. When we knocked down syt7 (~75% reduction in protein levels, Figure S5A-C) we observed complete blockade of the augmentation in spontaneous excitatory neurotransmission caused by ER Ca^{2+} depletion (Figure 4C). Moreover, there was a negative correlation between the

protein levels of syt7 and the increase in mEPSC frequency in syt7 KD group (Figure S5D). In syt1 KD neurons, when syt7 protein was also knocked down, the increase in mEPSC frequency during TG perfusion was also abolished (Figure 4D). Taken together, these results suggest that syt7 operates as the Ca^{2+} sensor mediating release in response to SOCE. This increase in spontaneous release depends on Ca^{2+} influx from the extracellular space since TG application in the absence of bath Ca^{2+} had no effect on mEPSC frequency or amplitude (Figure 4B), in accordance with our previous findings that CRAC channels and Ca^{2+} influx are necessary for SOCE regulation of excitatory spontaneous release.

Syt7 is a high-affinity Ca^{2+} sensor with slow kinetics for vesicle fusion, while syt1 is fast and has a lower Ca^{2+} affinity (Sugita et al., 2002). To understand the relevance of the presynaptic increase in Ca^{2+} triggered by SOCE in the context of the Ca^{2+} affinity of synaptotagmins, we performed live Ca^{2+} calibration and imaging experiments (Figure 4F-G, and see methods). Although GCaMP probes are not quantitative tools, changes in Ca^{2+} concentration can be estimated if a calibration curve is performed under the exact same experimental conditions (Figure S5E; and see Henderson et al., 2015). Using this approach, we estimated the increase in presynaptic Ca^{2+} concentration in control, syt7 KD and BTP2 treated (CRAC blocker, 300 nM) rat hippocampal neurons (Figure 4F-G). In control and syt7 KD neurons, ~50% of synapses showed an increase in presynaptic Ca^{2+} levels >1μM (and in average 25% of synapses showed Ca^{2+} concentration >2μM; mean Ca^{2+} increase = [1.6 ± 0.1] μM; Figure 4G). Pretreatment with BTP2 blocked the increase in presynaptic Ca^{2+}, with an average of only ~10% of synapses reaching concentrations above 2 μM (mean Ca^{2+} increase in BTP2 = [0.85 ± 0.05] μM Figure 4F-G). This result agrees with our previous finding of BTP2 blockade of TG-induced increase in mEPSC frequency (Figure 3H-I). Syt7 Ca^{2+} affinity (EC_{50}) was previously estimated to be ~1-2 μM, while syt1 affinity ranges ~10-20 μM (in chromaffin cells; Sugita et al., 2002). Thus, our estimation of SOCE-mediated increase in presynaptic Ca^{2+} indicates that Ca^{2+} concentration increases to levels around or above syt7 affinity, but in most synapses this may not be sufficient to activate syt1, supporting the premise that syt7 is the main Ca^{2+} sensor mediating excitatory spontaneous release triggered by SOCE.

To further investigate if Ca^{2+} binding to syt7 is necessary for its role in SOCE-dependent augmentation of spontaneous release, we performed rescue experiments using a mutated form of syt7 that has key acidic residues for Ca^{2+} binding neutralized (syt7 5DA mutation; Figure 5A-B and Figure S5F-G) (Bacaj et al., 2015). Syt7 5DA mutant protein is thus incapable of binding Ca^{2+}. While expression of wild-type (WT) shRNA-resistant syt7 fully rescued the syt7 KD phenotype (Figure 5C-E and G), syt7 5DA was unable to restore the SOCE-mediated increase in the frequency of mEPSC (Figure 5D-E and G). We also tested a recently described mutation in syt7 C2A domain, F167M/R231K (syt7 MK), that decreases syt7 affinity for phospholipids without affecting Ca^{2+} binding (Figure 5A-B and Figure S5F-G) (Voleti et al., 2017). Syt7 MK showed an intermediate phenotype, with an average 25% increase in mEPSC frequency after TG perfusion (Figure 5E) and ~60% of neurons still responding to TG (Figure 5G). This intermediate effect might reflect a partial reduction in membrane affinity upon Ca^{2+} binding by syt7, when compared to the more dramatic impact of 5DA mutation. While 5DA mutation completely abolishes Ca^{2+} binding, MK mutation might only lower it to values slightly under or close to the Ca^{2+} influx caused by TG (as

shown in Figure 4F-G) thus providing a more “probabilistic” response to SOCE activation. As previously shown, syt7 couples the increase in presynaptic Ca^{2+} to spontaneous release without affecting Ca^{2+} influx itself, since SOCE-mediated increase in presynaptic Ca^{2+} was intact in syt7 KD neurons (Figure 4F-G). Taken together, our results show that Ca^{2+} binding to syt7 is necessary for the increase in spontaneous release after SOCE activation at excitatory synapses.

Intact Ca^{2+}-binding sites are necessary for the clamping role of synaptotagmin-1 (Xu et al., 2009), indicating that it may be able to sense Ca^{2+} fluctuations at rest and prevent those fluctuations to impact spontaneous neurotransmission (putatively through competing with secondary Ca^{2+} sensors, see Xu et al., 2009). Due to its lower Ca^{2+} affinity, STM2 has been proposed to respond to small Ca^{2+} fluctuations in resting neurons and trigger SOCE, putatively participating in homeostatic control of neuronal Ca^{2+} levels (Gruszczynska-Biegala et al., 2011). Even though knocking out STIM2 had no effect on resting spontaneous excitatory neurotransmission (Figure 3C), removing STIM2 in neurons lacking syt1 rescued the classical syt1 phenotype, i.e. it reverted the increase in mEPSC frequency (dissociated mouse hippocampal neurons, Figure 6A-B and D). Accordingly, if syt1 KD neurons are pretreated with the CRAC inhibitor BTP2 (300 nM), resting mEPSC frequency was also considerably reduced (dissociated rat hippocampal neurons, Figure 6C-D). Both manipulations, STIM2 cKO and BTP2 treatment, blocked the increase in mEPSC frequency triggered by SOCE activation in syt1 KD neurons (Figure 6B-C and E), with no impact on mEPSC amplitude (Figure 6F). This surprising result indicates that syt1 normally tempers spontaneous release that might be caused by small Ca^{2+} fluctuations and SOCE activation under resting conditions, thus maintaining homeostatic levels of basal neurotransmission.

SOCE activation participates in the development of synaptic alterations during ER stress

The ER is the main intracellular store of Ca^{2+} and it participates in numerous signaling pathways. The ER is also the place where most of the proteins and lipids are synthesized, and protein folding check, modifications and transport start. Numerous neurodegenerative diseases involve aggregation of misfolded proteins and alterations in Ca^{2+} homeostasis, including Parkinson’s disease, Alzheimer’s disease, Huntington’s disease and prion disease (Pchitskaya et al., 2018; Popugaeva et al., 2018). These cellular abnormalities impact on ER function and lead to a process called ER stress, a pathway that initially restores ER metabolism but if activated for long periods it can lead to apoptosis. In neurons, chronic ER stress has been associated with the emergence of synaptic abnormalities and neurodegeneration (Hetz and Saxena, 2017; Pchitskaya et al., 2018). To investigate if presynaptic SOCE activation is involved in this pathological mechanism, we pharmacologically triggered ER stress in hippocampal neurons. Our group has previously shown that long term (24-72 h) treatment with tunicamycin (TM; a blocker of N-glycosylation) or TG causes chronic ER stress in neurons leading to a dramatic increase in spontaneous neurotransmission and impairing N-methyl-D-aspartate (NMDA) receptor-dependent postsynaptic plasticity responses (Nosyreva and Kavalali, 2010). Following the same experimental protocol, we incubated hippocampal neurons for 48h with either 5 μg/mL TM or 300 nM TG in the absence or presence of the SOCE blocker BTP2 (at 300 nM; Figure 7A-C). While induction of chronic ER stress with TG or TM led to a significant

increase in mEPSC frequency, but not amplitudes, abolishing Ca^{2+} influx trough CRAC channels with BTP2 partially reverted this phenotype (Figure 7B-C), indicating that SOCE activation may contribute to the alterations in neurotransmission observed during chronic ER stress. Since the Ca^{2+} sensor syt7 is the main molecule coupling SOCE to spontaneous release, we next assessed the effect of TM or TG in syt7 KD neurons (Figure 7A). Chronic ER stress had a reduced impact on spontaneous neurotransmission in neurons lacking syt7 (Figure 7A-C), indicating that a pathway involving ER stress, SOCE and syt7 participates in the dysregulation of spontaneous neurotransmission at excitatory synapses.

How does SOCE contribute to ER stress and the resulting neuronal alterations? A simple hypothesis would be that ER stress results in Ca^{2+} depletion from the ER lumen, activating SOCE. SOCE in turn would lead to increased synaptic levels of Ca^{2+} triggering spontaneous release through syt7. To test this hypothesis, we measured relative Ca^{2+} levels in presynaptic boutons (Figure 7D-E). Both pharmacological treatments, TM and TG, caused an increase in presynaptic Ca^{2+} content (Figure 7D-E) and this was reverted by co-incubation with the CRAC blocker BTP2 (Figure 7D-E). These results suggest that SOCE links ER stress to increased spontaneous neurotransmission via upregulation of presynaptic Ca^{2+} levels. As previously shown, the effects on neurotransmitter release are likely not due to apoptosis since chronic ER stress only caused a ~10% increase in neuronal death, and this was not reverted by BTP2 treatment (Figure S6A-B) (Nosyreva and Kavalali, 2010).

If cell homeostasis is not restored, chronic ER stress initiates the apoptosis cascade by upregulating the C/EBP homologous protein (CHOP; Figure 7F) (Nosyreva and Kavalali, 2010; Sano and Reed, 2013). The two pharmacological approaches used here, TG and TM, increased both the levels (Figure 7G) and the number of neurons (Figure 7H) expressing CHOP compared to control. Treatment with the SOCE-inhibitor BTP2 or knocking down syt7 could reduce, but not eliminate, the ER stress-mediated upregulation of CHOP (Figure 7F-H). Another downstream effector upregulated by ER stress is the protein disulfide isomerase (PDI). While PDI has beneficial effects in maintaining proteostasis during acute ER stress, prolonged increase of PDI during chronic ER stress has been reported to be detrimental (Perri et al., 2016). In our setting, chronic ER stress led to an increase in PDI levels in neurons treated with TM and TG (Figure 8A-B). This increase in PDI was partially prevented by addition of BTP2 (300 nM) to the culture media or by knocking-down syt7 (Figure 8A-B), indicating a protective role of SOCE/syt7 pathway blockade. One of the master regulators triggering several unfolded protein responses and ER stress related cascades is the ER resident binding immunoglobulin protein (BiP) (Pobre et al., 2018; Shah et al., 2015). BiP protein and its direct downstream effectors, IRE1α, PERK and ATF6, have all been found to be increased in neurodegenerative diseases, possibly as a protective response to the accumulation of misfolded proteins (although the positive or negative impact of this increase is still debated) (Hughes and Mallucci, 2019; Katayama et al., 2004; Shah et al., 2015). In dissociated hippocampal neurons, chronic ER stress caused an increase in BiP (Figure S6C-D) and IRα (Figure 8C-D) levels. This increase was not reverted by treating with BTP2 or knocking down syt7 (Figure 8C-D and Figure S6C-D). Taken together, our results indicate that downstream cascades activated by chronic ER stress can be exacerbated by SOCE activation, since blockade of CRAC or reduction of syt7 levels can partially revert the neurotransmission and molecular changes, but the upstream master signals triggering ER

stress response are not affected. Thus, SOCE may be a downstream pathway that participates and contributes, but does not per se cause, the neuronal dysfunctions resulting from chronic ER stress.

In conclusion, our results show that prolonged perturbations in ER Ca^{2+} levels or protein folding in hippocampal neurons leads to chronic ER stress. This chronic stress is coupled to SOCE. SOCE activation leads to a sustained increase in presynaptic Ca^{2+} content enhancing spontaneous excitatory neurotransmission via syt7. We propose that this increase in basal SOCE and glutamate release may contribute and exacerbate synaptic dysfunction associated with neurodegeneration.

Discussion

In this study, we used TG to acutely perturb ER luminal Ca^{2+} levels in hippocampal neurons and investigate the presence and the role of SOCE in presynaptic terminals. We found that SOCE, in a STIM2 and CRAC dependent manner, can transiently increase presynaptic Ca^{2+} levels leading to a robust augmentation of spontaneous release of neurotransmitters through the Ca^{2+} sensor syt7. This mechanism regulates primarily spontaneous neurotransmission, not evoked, and occurs exclusively at excitatory synapses, as inhibitory miniature currents were unaffected by these manipulations. Given that ER Ca^{2+} homeostasis has been implicated in numerous neurodegenerative diseases, we also explored the role of presynaptic SOCE in previously described ER stress-driven neuronal signaling. We found that pharmacological inhibition of SOCE, with the Orai antagonist BTP2, or abolishment of the SOCE-dependent increase in spontaneous neurotransmission through elimination of syt7, both partially reduce the alterations in neurotransmission and the activation of pro-apoptotic cascades in neurons after ER stress induction.

STIM proteins sense ER Ca^{2+} through a luminal EF-hand motif so that reductions in Ca^{2+} concentration trigger a conformational change leading to STIM oligomerization and accumulation at ER-plasma membrane junctions. At these junctions, STIM oligomers sequester and cluster plasma membrane Orai Ca^{2+} channels thus gating their opening (Soboloff et al., 2012). Since the discovery of SOCE pathway (Putney, 1990) and the corresponding Ca^{2+} current (Hoth and Penner, 1992), followed by the more recent discovery of STIM (Liou et al., 2005; Roos et al., 2005) and Orai proteins (Feske et al., 2006), SOCE has been implicated in the regulation of Ca^{2+} homeostasis and Ca^{2+} signaling in numerous cell types and organisms, participating in processes as diverse as the innate and adaptive immune responses, muscle contraction in lungs and heart, bone maturation and tumor malignancy (Soboloff et al., 2012). STIM and Orai proteins are also expressed throughout the nervous system and have been implicated in Ca^{2+} homeostasis in neurons (Wegierski and Kuznicki, 2018; Zhang and Hu, 2020).

The physiological role of SOCE in neurotransmission and neuronal homeostasis has only recently started to be uncovered. At the postsynaptic sites, neuronal SOCE provides Ca^{2+} signals that facilitate the maturation and stabilization of dendritic spines (Korkotian et al., 2017; Sun et al., 2014; Zhang et al., 2015) and it may contribute to NMDA receptor and α-amino-3-hydroxy-5-methyl-4-isoxazolepropionic acid (AMPA) receptor mediated signaling

(Baba et al., 2003; Garcia-Alvarez et al., 2015b; Gruszczynska-Biegala et al 2016) This modulation of dendritic signaling and morphology may be primarily driven by STIM2 and Orai1, and it positively regulates excitatory spontaneous neurotransmission, long-term potentiation and some types of hippocampal-dependent memory processes (Garcia-Alvarez et al., 2015a; Garcia-Alvarez et al., 2015b; Maneshi et al., 2020; Yap et al., 2017). Accordingly, we observed a small increase in mEPSC amplitude in STIM2 cKO neurons, supporting a role for STIM2 in postsynaptic levels and function of AMPARs. In addition, we show that STIM2 modulates presynaptic spontaneous glutamate release in response to SOCE, whereas STIM1 may impact resting presynaptic and postsynaptic properties, since both frequency and amplitude of mEPSCs are reduced in STIM1 KD neurons. Overexpression of STIM2 and Orai1 has only minor impact on basal (evoked) neurotransmission and behaviour in mice (interestingly, some sex-related differences were observed) (Maciąg et al., 2019; Majewski et al., 2020). This occurs without changes in basal neuronal Ca^{2+} levels or inhibitory neurotransmission, but with increased SOCE response and altered spontaneous excitatory neurotransmission, indicating that our findings agree with *in vivo* models. Postsynaptic effects of STIM1 and STIM2 seem to be opposite, since resting amplitudes of excitatory miniature events are decreased in STIM1 KD neurons and the opposite is observed in STIM2 KD neurons. In line with this notion of differential roles of STIM1 and 2, it was recently reported that STIM1 responds to calcium fluctuations during neuron development regulating dendritic maturation whereas STIM2 becomes prominent in adult cultured hippocampal neurons where it may mediate SOCE (Kushnireva et al., 2021) and impact on dendritic spine function and morphology as discussed above. Further research is necessary to elucidate the molecular underpinning and physiological significance of these differences. Presynaptically, STIM1 isoform has been proposed to be core modulatory component of the ER remodeling and Ca^{2+} signaling cascades involved in axonal growth and pathfinding during neuronal development (Mitchell et al., 2012; Pavez et al., 2019; Shim et al., 2013). More recently, STIM1 and ER Ca^{2+} content have also been implicated in the regulation of the probability of neurotransmitter release in hippocampal neurons (de Juan-Sanz et al., 2017). Release of Ca^{2+} from the stores and depletion of Ca^{2+} from the stores with the subsequent opening of CRAC channels have both been shown to trigger spontaneous excitatory neurotransmitter release in hippocampal and cortical brain slices (Emptage et al., 2001; Simkus and Striker, 2002; but also see Carter et al., 2002). SOCE activation can also increase excitability in dorsal horn and dorsal root ganglion neurons (Dou et la., 2018; Wei et al., 2017). Inhibitory spontaneous neurotransmission, however, was shown to be impervious to SOCE activation, Ca^{2+} release from the ER (Lim et al., 2003) or changes in Orai protein levels (Maciąg et al., 2019). Our results corroborate and expand these findings, by showing that the selective SOCE modulation of excitatory neurotransmission is probably due to enrichment of STIM2 protein in glutamatergic synapses. We also uncover the mechanism coupling presynaptic SOCE with spontaneous release at excitatory hippocampal synapses, through the activation of STIM2 and CRAC. Due to its high Ca^{2+} affinity, STIM2 was previously proposed to activate SOCE in response to basal fluctuations in Ca^{2+} concentration (Gruszczynska-Biegala and Kuznicki, 2013). Based on our results, these fluctuations could lead to increases in spontaneous neurotransmission, but this is prevented by the clamping effect of syt1, thus maintaining basal homeostatic level of release. The importance of syt1-mediated clamping of

spontaneous release and the specific involvement of STIM2 is revealed by the occlusion, or apparent rescue, effect of knocking out STIM2 in syt1 KD neurons, which reduces the abnormally high frequency of spontaneous fusion classically observed in synapses lacking syt1.

When neuronal Ca^{2+} homeostasis is perturbed by reducing ER Ca^{2+} levels, the control of syt1 is surpassed and another Ca^{2+} sensor with higher affinity, syt7 is activated by the Ca^{2+} influx through SOCE and it triggers neurotransmitter release. Syt7 was previously shown to clamp spontaneous release, being able to revert the increased miniature frequency in syt1 knock out neurons (Bacaj et al., 2013). Thus, our results show that similar to syt1, syt7 can have a dual role clamping and mediating spontaneous synaptic vesicle fusion (see Xu et al., 2009). In the future, it would be interesting to explore and compare the role of STIMs and SOCE activation in other, non-hippocampal synaptic circuits with different intrinsic neurotransmission properties and endogenous levels of syt1 and syt7 (Iremonger and Bains, 2007; Turecek and Regehr, 2019). Our results show that the extent of mEPSC frequency increase after SOCE activation correlates with the levels of syt7. Thus, we surmise that ER Ca^{2+} dynamics may be linked to release dynamically and differentially at synapses with varying levels of distinct synaptotagmin isoforms, and this variability in turn may lead to diverse plasticity and signaling properties with putative roles in different forms of memory and neuronal dysfunction. Accordingly, different forms of neurotransmission may be linked to different sources of Ca^{2+} (Courtney et al., 2018; Wen et al., 2013), indicating that our findings are only the beginning in understanding the role in ER-related Ca^{2+} signaling in neurotransmission.

Cytoplasmic and ER Ca^{2+} imbalances may result from prolonged high-frequency activity, excitotoxicity, ischemia or neurodegeneration (Bodalia et al., 2013; Power et al., 2005; Pozzo-Miller et al., 1997; Rusakov and Fine, 2003). For neurodegenerative disorders in particular, defects in postsynaptic Ca^{2+} homeostasis and SOCE regulation have been associated with the progression of neuronal deficits, including Huntington, Parkinson and Alzheimer's diseases (Pchitskaya et al., 2018; Popugaeva et al., 2018) (also see Zhang and Hu, 2020 for a review on SOCE and brain pathologies). Moreover, activation of the SOCE pathway postsynaptically has been proposed as a potential target for preventing memory loss in Alzheimer's disease (Sun et al., 2014; Zhang et al., 2015). ER stress due to unfolded proteins accumulation and Ca^{2+} dysregulation is a common component of these neurodegenerative diseases. In our experiments we could show that pharmacological induction of chronic ER stress, either through an unfolded protein response (using TM) or through prolonged ER Ca^{2+} depletion (using TG), leads to activation of the unfolded protein response and pro-apoptotic cascades in neurons, as revealed by BiP, IRE1α, PDI and CHOP upregulation, and increases basal presynaptic Ca^{2+} levels and spontaneous excitatory neurotransmission (also see Nosyreva and Kavalali, 2010). In the adult nervous system, the levels of spontaneous neurotransmission modulate network excitability, signaling and different forms of plasticity (Kavalali, 2015). In consequence, the sustained increase in spontaneous glutamate release observed during chronic ER stress may have a critical impact in network firing properties and information processing, contributing to the deterioration of neural circuits. A recent report found increased axonal Ca^{2+} waves and augmented spontaneous glutamate release in a mouse model of Huntington's disease, proposing

presynaptic release properties as a relevant component in the etiology of neurotransmission deficits (Mackay et al., 2020). Accordingly, blocking postsynaptic NMDA receptors reverts the increase in ER stress related signaling molecules and in excitatory neurotransmission (using the same chronic ER stress model used here; Nosyreva and Kavalali, 2010), indicating that defects in glutamatergic neurotransmission can propagate through the neuronal network via spontaneous neurotransmission. Taken together with our results, this earlier finding indicates that presynaptic increase in SOCE leads to accumulation of Ca^{2+} in the terminal and augments glutamate release via syt7 leading to activation of postsynaptic glutamate receptors and exacerbation of deficits in the downstream neurons. The pathway that we uncovered plays a central role, linking ER stress to presynaptic STIM2/Orai activation, increase in presynaptic Ca^{2+} levels and syt7-mediated increase in spontaneous neurotransmission. Blockade of this pathway, either through inhibiting SOCE or its downstream effector syt7, partially ameliorates the harmful impact of chronic ER stress in neuronal survival and neurotransmission. This neuroprotective effect of SOCE/STIM2 elimination was also observed during ischemia, where SOCE reduction via knocking-out STIM2 reduces Ca^{2+} accumulation in neurons and increases neuron survival both *in vitro* and *in vivo* (Berna-Erro et al., 2009). Interestingly, under these conditions elimination of STIM1 had no effect.

In conclusion, our results reveal a previously uncharacterized presynaptic SOCE pathway that regulates spontaneous neurotransmission at excitatory synapses. These findings also implicate presynaptic STIM2/Orai/syt7 as a contributing mechanism in the progression of synaptic and neuronal deficits upon chronic ER stress. These results provide new insight into presynaptic mechanisms linking intercellular Ca^{2+} stores to neurotransmitter release that may play a role in neurodegenerative disorders.

STAR Methods.

RESOURCE AVAILABILITY

Lead Contact—Further information and requests for resources and reagents should be directed to and will be fulfilled by the Lead Contact, Ege T. Kavalali, Department of Pharmacology, Vanderbilt University, Nashville, TN 37240-7933, USA. Phone: 615-343-5480 ege.kavalali@vanderbilt.edu

Material Availability—All plasmids used in the present manuscript are available for sharing via request to Ege T. Kavalali (ege.kavalali@vanderbilt.edu) or Natali L. Chanaday (natali.chanaday@vanderbilt.edu).

Data and Code Availability—This study did not generate any unique code.

EXPERIMENTAL MODEL AND SUBJECT DETAILS

Primary mouse and rat hippocampal cultures—Dissociated hippocampal cultures from postnatal day 2-3 Sprague-Dawley rats of both sexes were used for all the experiments. To prepare STIM2 cKO cultures, postnatal day 0-1 STIM2 fl/fl C57BL/6 mice of both sexes were used.

All experiments were performed following protocols approved by the UT Southwestern Institutional Animal Care and Use Committee and the Vanderbilt University Medical Center Institutional Animal Care and Use Committee.

Sample size estimation—The approach we used for this research is hypothesis free, we did not have prior knowledge of the type of result or values we were going to obtain or of the magnitude of the effect of the tested treatments or genetic manipulations. For that reason, prior statistical power analysis and sample-size estimation was not possible. Nevertheless, the number of experiments and samples needed can be inferred from previous, similar experiments performed in our lab, using the same type of cultures. Assuming the reproducibility of experimental conditions and settings, we estimated that a minimum of 2 independent cultures with 2 coverslips for fluorescence experiments (with ~50-100 presynaptic boutons per coverslip analyzed) or 3 independent cultures with 3 coverslips for electrophysiology experiments (1 whole cell recordings per coverslip) per experimental group was enough for significance testing and finding the presence or absence of differences or tendencies among groups. Based on the variances and tendencies observed, in some cases the addition of extra experiments was decided.

Experimental groups were pre-designed based on the treatment (e.g. treated vs untreated control or knock-down/mutated vs WT control). All experimental groups for each particular data set were present in each experiment and measured in a random order under the exact same conditions (i.e. buffers, solutions, drugs and other reagents as well as temperature, culture age and other conditions were the same for all samples).

METHOD DETAILS

Dissociated hippocampal cultures—Postnatal day 2-4 Sprague-Dawley rats or postnatal day 0-1 STIM2 fl/fl C57BL/6 mice were used for the experiments. Both hippocampi were dissected in sterile conditions and posteriorly dissociated using 10 mg/ml trypsin and 0.5 mg/ml DNAase for 10 min at 37°C. After careful trituration using a P1000 pipette, cells were resuspended to a concentration of 1 pup per 12 coverslips and plated onto 12 mm coverslip coated with 1:50 MEM:Matrigel solution. Basic growth medium consisted of MEM medium (no phenol red), 5 g/l D-glucose, 0.2 g/l $NaHCO_3$, 100 mg/l transferrin, 5% of fetal bovine serum, 0.5 mM L-glutamine, 2% B-27 supplement, and 2–4 μM cytosine arabinoside. Cultures were kept in humidified incubators at 37°C and gassed with 95% air and 5% CO_2.

Acute hippocampal slices—P50-P60 mice of both sexes were sacrificed, brains were immersed in a 95% O_2 / 5% CO_2 aerated ice-cold NMDG-HEPES cutting solution including (in mM): 92 NMDG, 2.5 KCl, 1.25 NaH_2PO_4, 30 $NaHCO_3$, 20 HEPES, 25 glucose, 2 thiourea, 5 Na-ascorbate, 3 Na-pyruvate, 0.5 $CaCl_2$-$2H_2O$, and 10 $MgSO_4$-7H2O, titrated pH to 7.3–7.4 with 17 mL +/− 0.5 mL of 5 M hydrochloric acid and 300 μm thick fresh coronal slices containing the hippocampus were obtained with vibratome and transferred to 95% O_2 / 5% CO_2 aerated artificial cerebrospinal fluid (aCSF) containing (in mM): 119 NaCl, 25 NaHCO3, 11 dextrose, 2.5 KCl, 1.25 $MgCl_2$, 2 $CaCl_2$ and 1.25 NaH_2PO4. The sections were incubated in this solution for approximately 45 minutes in the room

temperature and then, placed in the recording chamber. Recording solution also contained TTX (1μM) and $GABA_A$ blocker (PTX 10 μM) to isolate mEPSCs.

Whole-cell voltage clamp recordings were performed on CA1 pyramidal neurons using electrodes with 4-5 MΩ tip resistances with pipette solution containing (in mM): 125 CsCl, 5 NaCl, 10 HEPES, 0.6 EGTA, 4 Mg-ATP, 0.3 Na_2GTP, 10 lidocaine N-ethyl bromide (QX-314), pH 7.35 and 290 mOsm l-1. The holding potential for voltage clamp recordings was −70 mV. MultiClamp 700B Amplifier (Molecular Devices, San Jose, CA) and Axon™ pCLAMP™ 11 software (Molecular Devices, San Jose, CA) were used to obtain and analyze data. For recordings, following whole cell voltage clamp, CA1 pyramidal neurons were recorded for 1.5 minutes for baseline activity in 2 mM Ca^{2+}, bath solution was then rapidly replaced with 0 mM Ca^{2+} using fast perfusion for 1 minute followed by 2 mM Ca^{2+} with 1 μM TG for 10 minutes.

Pharmacological treatments—The SOCE inhibitors BTP2 and SKF 96365 (at 300 nM and 30 μM concentration, respectively) were preincubated in the culture media for 45 min before the experiments, and they were also present in all the bath solutions. For induction of chronic ER stress, sterile solutions of TG and TM (at 300 nM and 5 μg/mL final concentration, respectively) were added to the culture media and incubated for 48 h. For all drugs, stock solutions were used up to 6 months after preparation and aliquoted into small volumes (to avoid repeated freeze and thaw). Working solutions were prepared freshly before each experiment.

Cloning—Previously described point mutations on syt7 (Bacaj et al., 2015; Voleti et al., 2017) were generated using classic PCR techniques. Rat syt7 cDNA sequence was used (U20106) and silent point mutations were performed in the region recognized by the shRNA to render it shRNA-resistant (described in detail in Bacaj et al., 2013). All constructs were subcloned into pFU-GW lentiviral vector from Addgene (plasmid # 14883). shRNAs targeting STIM1 and STIM2 were subcloned into L307 vector from Dr. Thomas C. Sudhof laboratory.

Lentiviral infection—The VGluT1-pHluorin construct was a gift from Drs. R.H. Edwards and S.M. Voglmaier (University of California, San Francisco) (Voglmaier et al., 2006). shRNA against synaptotagmin-1 and synaptotagmin-7 inserted in L307 plasmid were a gift from Dr. Thomas Südhof (Stanford University) (Xu et al., 2012, Bacaj et al., 2013). Previously used sequences of the Cre recombinase and GFP were inserted into lentiviral FUGW vector (see Lin et al., 2018). Lentiviruses were produced in HEK293T cells by contransfection of pFUGW transfer vectors and 3 packaging plasmids (pCMV-VSV-G, pMDLg/pRRE, pRSV-Rev) using Fugene 6 transfection reagent. The supernatants of the cultures were collected 72 hours after the transfection and clarified by centrifugation (2500 rpm 15 min), and subsequently used for infection of DIV 4 hippocampal neurons. All experiments were performed on 18–20 DIV cultures when synapses were mature and lentiviral expression of constructs of interest was optimal (Mozhayeva et al., 2002; Deak et al., 2006). All experiments were performed following protocols approved by the UT Southwestern Institutional Animal Care and Use Committee and the Vanderbilt University Medical Center Institutional Animal Care and Use Committee.

Electrophysiology (neuron cultures)—Cultured pyramidal neurons at 16 to 20 DIV were used for whole cell recordings at a clamped voltage of −70 mV by means of Axopatch 200B and Clampex 8.0 software (Molecular Devices), filtering at 1 kHz and sampling at 5 kHz. Only experiments with access resistance 5–20 MΩ were considered for analysis. All recordings were performed at room temperature. The cells were visualized using a Nikon DIAPHOT 200 microscope. The internal pipette solution contained 115 mM $CsMeSO_3$, 10 mM CsCl, 5 mM NaCl, 10 mM HEPES, 0.6 mM EGTA, 20 mM tetraethylammonium chloride, 4 mM Mg-ATP, 0.3 mM Na_2GTP and 10 mM QX-314 (lidocaine N-ethyl bromide). The final solution was adjusted to pH 7.3 and 305-310 mOsM. Final resistance of the electrode tips was ~ 2-5 MΩ. For all experiments, the extracellular solution was a modified Tyrode's solution containing 150 mM NaCl, 4 mM KCl, 10 mM glucose, 10 mM HEPES and 2 mM $MgCl_2$, adjusted to pH 7.4 and 315-320 mOsM. To isolate inhibitory postsynaptic currents, agonists of ionotropic glutamate receptors were added: 10 μM 6-cyano-7-nitroquinoxaline-2,3-dione (CNQX) and 50 μM aminophosphonopentanoic acid (AP-5). To isolate excitatory currents (AMPA-mediated) 50 μM AP-5 and 50 μM picrotoxin (PTX, ionotropic GABA receptor inhibitor) were added to the bath solution. To elicit evoked responses, electrical stimulation was delivered through parallel platinum electrodes with a constant current unit (WPI A385) set at 35 mA. Spontaneous activity (mIPSCs and mEPSCs) were recorded with the addition of 1 μM TTX. For detection, a threshold of 8 pA in amplitude (rise/decay time <5ms/20ms; peak area>25μs*pA) was used for mESPC and 12 pA (rise/decay time <10ms/40ms; peak area>50μs*pA) for mIPSC. Analysis was performed with MiniAnalysis.

Western blotting—Western blots were performed as described in Nosyreva and Kavalali (2010). Primary antibody dilutions: anti-GDI 1:2000, anti-GAPDH 1:20000, anti-syt7 1:500, anti-syt1 1:1000, anti-STIM1 1:1000, anti-STIM2 1:1000, anti-IRE1α 1:500. Immunoreactive bands were visualized by near-infrared fluorescence using an Odyssey scanner (LI-COR) and analyzed using GelAnalyzer2010 software. Protein levels were normalized to GDI or GAPDH loading controls. Syt1, syt7 and STIM2 antibodies were checked by our laboratory using respective KD samples (they were also validated previously by others, see references in Key Resources Table). When possible, we purchase only KO-validated antibodies by the corresponding company.

Immunofluorescence and colocalization—Neuron cultures were fixed for 15 min in PBS containing 1% para-formaldehyde (PFA) and 7.5% sucrose. Posteriorly, coverslips were incubated for 15 min in 50 mM glycine in PBS to reduce autofluorescence and permeabilized for 10 min using 0.0075% digitonin in PBS. Samples were blocked with 1% bovine serum albumin (BSA), 3% goat serum and 0.2% fish gelatin in PBS for 1 h at room temperature. Antibodies were diluted in blocking buffer and incubated over-night at 4 °C in a humid chamber. Antibodies against MAP2, Syn1, BiP and CHOP were used at 1:1000 dilution, anti-Tau and anti-PDI at 1:500, anti-PSD95 at 1:100, and anti-STIM2 was used at 1:50 dilution. Alexa conjugated secondary antibodies (1:1000) were used to label the cells and then coverslips were imaged using an LSM 510 META confocal microscope (Carl Zeiss) with a 63X (NA1.4) objective. Z-stack images were acquired every 500 nm, with 1 μM optical z-section. Object-based colocalization was analyzed using Fiji (NIH). Basically,

to generate the 3D objects images were background subtracted (Rolling ball of 100 px), thresholded (using Moments method), binarized and segmented (based on shape and size). Objects were detected using the 3D object counter feature in Fiji. For colocalization, binary images of each channel (color) were multiplied, and objects in the resulting image (i.e. colocalizing regions only) were compared to the original channels. Positive colocalization was defined as an overlap of more than 50 voxels of two colors in the same object (calibration: 1 voxel = 0.143 × 0.143 × 1 μm). This was performed in an automated fashion using a custom made macro for Fiji. The detection parameters were adjusted using a positive control with 100% colocalization (synasin-1 and synaptobrevin-2 immunolabeling), and a negative control with little colocalization (VGluT1 and VGAT immunolabeling). For 2-color 2D-STED the same labeling protocol was used, and images were taken using a STEDYCON microscope (Aberior Instruments) and NIS-Elements software for deconvolution (Nikon Instruments). Individual presynaptic boutons were selected and analyzed using Fiji (NIH).

Fluorescence live imaging—Cultured hippocampal neurons at 18–20 DIV infected with either Sy2-GCaMP6s, ER-GCaMP6-150 or VGluT1-pHluorin were used for the imaging experiments. The modified Tyrode's buffer from above containing 0 or 2 mM Ca^{2+} was used with 1 μM TTX. Fluorescence was recorded using a Nikon Eclipse TE2000-U microscope (Nikon) and an Andor iXon+ back-illuminated EMCCD camera (Model no. DU-897E-CSO-#BV). For illumination we used a Lambda-DG4 illumination system (Sutter instruments) with a FITC emission filter. Images were acquired at 10 Hz and only for pHluorin experiments binning of 4 by 4 was used to optimize the signal-to-noise ratio. Maximal fluorescence signal was detected by perfusing 90 mM KCl or 500 μM ionomycin for Syb2-GCaMP6s and ER-GCaMP6-150, or 50 mM NH_4Cl for VGluT1-pHluorin, and it was also used to draw the regions of interest (ROI) around presynaptic boutons and/or neuron cell bodies. Images were analyzed using Fiji (NIH) and spontaneous fusion of synaptic vesicles was analyzed using a Matlab script previously described (Chanaday and Kavalali, 2018a).

Calibration of syb2-GCaMP6s—Cultured hippocampal neurons at 18–20 DIV infected with Sy2-GCaMP6s were placed in a recording chamber containing the modified Tyrode's solution mentioned above. The calibration in live neurons was performed based on a previous method (Henderson et al., 2015), with modifications. Microscope settings were similar as described above. Baseline was recorded for 2 min in Tyrode's buffer containing 2 mM Ca^{2+} (this is F_0). Then, the following solutions, prepared in Ca^{2+}-free Tyrode's containing TTX, were sequentially perfused in ascending order of Ca^{2+} concentration: 0 mM Ca^{2+} + 200 μM EGTA, 0.1 μM Ca^{2+}, 0.3 μM Ca^{2+}, 0.6 μM Ca^{2+}, 1 μM Ca^{2+}, 10 μM Ca^{2+}, 100 μM Ca^{2+}, 250 μM Ca^{2+}, 500 μM Ca^{2+}. All these solutions also contained diluted Ca^{2+} ionophores: 20 μM A23187 and 10 μM ionomycin. Ionophores concentration was set to be low enough to preserve cell viability while still producing quick Ca^{2+} exchange. 3 min of incubation was allowed in between each perfusion, to reach Ca^{2+} equilibrium, and then fluorescence was recorded for 1 min (all recordings in each coverslip were captured from the exact same field, so individual presynaptic boutons could be tracked). We observed a loss of cell viability for Ca^{2+} solutions above 250 μM, so data points from 0 to 100 μM Ca^{2+} were used for the standard curve. The mean fluorescence at each Ca^{2+} concentration was normalized to baseline fluorescence (F/F_0). F/F_0 was then plotted as a function of the

logarithm (base 10) of Ca^{2+} concentration (in μM) and fitted with a line. Using the same set of cultures, and in the same day, the live imaging experiments testing TG were performed, and the amplitude of the signal in each presynaptic bouton (calculated as $\Delta F/F_0$) was interpolated to the standard curve and Ca^{2+} concentration was estimated.

Cell viability assay—LIVE/DEAD kit (Molecular Probes) was used following the manufacturer instructions. Briefly, hippocampal cultures were incubated with 6 μM ethidium homodimer-1 and 2 μM calcein-AM in modified Tyrode's buffer for 45 min at room temperature and imaged using an LSM 510 META confocal microscope (Carl Zeiss) with a 40X objective.

QUANTIFICATION AND STATISTICAL ANALYSIS

Detailed statistical information for each experiment is provided in the figure legends. Briefly, the Kolmogorov–Smirnov (K-S) test was used to determine differences in cumulative probability histograms when comparing 2 groups, for 3 or more groups histograms were compared using Kruskal-Wallis analysis of medians and Dunn's multiple comparison post-test. For parametrically-distributed data, t-test and one-way or two-way ANOVA with appropriate multiple comparison post-tests (Dunnet, Sidak or Tukey) were employed, depending on the number of groups and treatments. Detailed N, mean and SEM for each group and experiment, along with p-values are informed in Table 1. Violin plots show the full distribution of all experimental data, central dashed line shows the mean value. Bar graphs show mean ± SEM. Effort was directed to minimize the number of animals used for the experiments.

Supplementary Material

Refer to Web version on PubMed Central for supplementary material.

Acknowledgements

We would like to thank Dr Nathan Grega-Larson (Nikon Instruments, Vanderbilt University) for his assistance with 2D-STED microscopy. This work was supported by grants from the National Institute of Mental Health (MH66198-19) to ETK, from the National Institute of Aging (AG055577-01) to IB and ETK, from the National Institute of Diabetes and Digestive and Kidney Diseases (R01DK126740) to DA and a NARSAD young investigator award to NLC. IB holds the Carl J. and Hortense M. Thomsen Chair in Alzheimer's Disease Research.

References

Baba A, Yasui T, Fujisawa S, Yamada RX, Yamada MK, Nishiyama N, Matsuki N, and Ikegaya Y (2003). Activity-evoked capacitative Ca2+ entry: implications in synaptic plasticity. J Neurosci 23, 7737–7741. [PubMed: 12944501]

Bacaj T, Wu D, Burre J, Malenka RC, Liu X, and Sudhof TC (2015). Synaptotagmin-1 and -7 Are Redundantly Essential for Maintaining the Capacity of the Readily-Releasable Pool of Synaptic Vesicles. PLoS Biol 13, e1002267. [PubMed: 26437117]

Bacaj T, Wu D, Yang X, Morishita W, Zhou P, Xu W, Malenka RC, and Südhof TC (2013). Synaptotagmin-1 and synaptotagmin-7 trigger synchronous and asynchronous phases of neurotransmitter release. Neuron 80(4), 947–959. [PubMed: 24267651]

Berna-Erro A, Braun A, Kraft R, Kleinschnitz C, Schuhmann MK, Stegner D, Wultsch T, Eilers J, Meuth SG, Stoll G, and Nieswandt B (2009). STIM2 regulates capacitive Ca2+ entry in neurons and plays a key role in hypoxic neuronal cell death. Science signaling, 2(93), ra67. [PubMed: 19843959]

Bezprozvanny I, and Kavalali ET (2020). Presynaptic endoplasmic reticulum and neurotransmission. Cell Calcium 85, 102133. [PubMed: 31812114]

Bird GS, DeHaven WI, Smyth JT, and Putney JW Jr (2008). Methods for studying store-operated calcium entry. Methods (San Diego, Calif.), 46(3), 204–212.

Bodalia A, Li H and Jackson M (2013). Loss of endoplasmic reticulum Ca2+ homeostasis: contribution to neuronal cell death during cerebral ischemia. Acta Pharmacol Sin 34, 49–59. [PubMed: 23103622]

Brandman O, Liou J, Park WS, and Meyer T (2007). STIM2 is a feedback regulator that stabilizes basal cytosolic and endoplasmic reticulum Ca2+ levels. Cell, 131(7), 1327–1339. [PubMed: 18160041]

Carter AG, Vogt KE, Foster KA, and Regehr WG. (2002). Assessing the role of calcium-induced calcium release in short-term presynaptic plasticity at excitatory central synapses. J Neurosci 22, 21–28. [PubMed: 11756484]

Chanaday NL, and Kavalali ET (2018a). Optical detection of three modes of endocytosis at hippocampal synapses. eLife, 7, e36097. [PubMed: 29683423]

Chanaday NL, and Kavalali ET (2018b). Presynaptic origins of distinct modes of neurotransmitter release. Current opinion in neurobiology 51, 119–126. [PubMed: 29597140]

Courtney NA, Briguglio JS, Bradberry MM, Greer C, and Chapman ER (2018). Excitatory and Inhibitory Neurons Utilize Different Ca2+ Sensors and Sources to Regulate Spontaneous Release. Neuron, 98(5), 977–991.e5. [PubMed: 29754754]

de Juan-Sanz J, Holt GT, Schreiter ER, de Juan F, Kim DS, and Ryan TA (2017). Axonal Endoplasmic Reticulum Ca(2+) Content Controls Release Probability in CNS Nerve Terminals. Neuron 93, 867–881 e866. [PubMed: 28162809]

Deàk F, Shin OH, Kavalali ET, and Südhof TC (2006). Structural determinants of synaptobrevin 2 function in synaptic vesicle fusion. The Journal of neuroscience : the official journal of the Society for Neuroscience, 26(25), 6668–6676. [PubMed: 16793874]

Dou Y, Xia J, Gao R, Gao X, Munoz FM, Wei D, Tian Y, Barrett JE, Ajit S, Meucci O, Putney JW Jr, Dai Y, & Hu H (2018). Orai1 Plays a Crucial Role in Central Sensitization by Modulating Neuronal Excitability. The Journal of neuroscience : the official journal of the Society for Neuroscience, 38(4), 887–900. [PubMed: 29229703]

Dull T, Zufferey R, Kelly M, Mandel RJ, Nguyen M, Trono D, & Naldini L (1998). A third-generation lentivirus vector with a conditional packaging system. Journal of virology, 72(11), 8463–8471. [PubMed: 9765382]

Emptage NJ, Reid CA, and Fine A (2001). Calcium stores in hippocampal synaptic boutons mediate short-term plasticity, store-operated Ca2+ entry, and spontaneous transmitter release. Neuron 29, 197–208. [PubMed: 11182091]

Feske S, Gwack Y, Prakriya M, Srikanth S, Puppel SH, Tanasa B, Hogan PG, Lewis RS, Daly M, and Rao A (2006). A mutation in Orai1 causes immune deficiency by abrogating CRAC channel function. Nature 441, 179–185. [PubMed: 16582901]

Garcia-Alvarez G, Lu B, Yap KA, Wong LC, Thevathasan JV, Lim L, Ji F, Tan KW, Mancuso JJ, Tang W, Poon SY, Augustine GJ, and Fivaz M (2015). STIM2 regulates PKA-dependent phosphorylation and trafficking of AMPARs. Molecular biology of the cell, 26(6), 1141–1159. (b). [PubMed: 25609091]

Garcia-Alvarez G, Shetty MS, Lu B, Yap KA, Oh-Hora M, Sajikumar S, Bichler Z, and Fivaz M (2015). Impaired spatial memory and enhanced long-term potentiation in mice with forebrain-specific ablation of the Stim genes. Frontiers in behavioral neuroscience, 9, 180. (a). [PubMed: 26236206]

Gruszczynska-Biegala J, and Kuznicki J (2013). Native STIM2 and ORAI1 proteins form a calcium-sensitive and thapsigargin-insensitive complex in cortical neurons. J Neurochem 126, 727–738. [PubMed: 23711249]

Gruszczynska-Biegala J, Pomorski P, Wisniewska MB, and Kuznicki J (2011). Differential roles for STIM1 and STIM2 in store-operated calcium entry in rat neurons. PLoS One 6, e19285. [PubMed: 21541286]

Gruszczynska-Biegala J, Sladowska M, and Kuznicki J (2016). AMPA Receptors Are Involved in Store-Operated Calcium Entry and Interact with STIM Proteins in Rat Primary Cortical Neurons. Front Cell Neurosci 10, 251. [PubMed: 27826230]

Henderson MJ, Baldwin HA, Werley CA, Boccardo S, Whitaker LR, Yan X, Holt GT, Schreiter ER, Looger LL, Cohen AE, Kim DS, and Harvey BK (2015). A Low Affinity GCaMP3 Variant (GCaMPer) for Imaging the Endoplasmic Reticulum Calcium Store. PloS one, 10(10), e0139273. [PubMed: 26451944]

Hetz C, and Saxena S (2017). ER stress and the unfolded protein response in neurodegeneration. Nat Rev Neurol 13, 477–491. [PubMed: 28731040]

Horton AC, and Ehlers MD (2004). Secretory trafficking in neuronal dendrites. Nat Cell Biol 6, 585–591. [PubMed: 15232591]

Hoth M, and Penner R (1992). Depletion of intracellular calcium stores activates a calcium current in mast cells. Nature 355, 353–356. [PubMed: 1309940]

Hughes D and Mallucci GR (2019). The unfolded protein response in neurodegenerative disorders - therapeutic modulation of the PERK pathway. FEBS J. 286(2):342–355. [PubMed: 29476642]

Iremonger KJ, and Bains JS (2007). Integration of asynchronously released quanta prolongs the postsynaptic spike window. J Neurosci 27(25), 6684–6691. [PubMed: 17581955]

Katayama T, Imaizumi K, Manabe T, Hitomi J, Kudo T, Tohyama M (2004). Induction of neuronal death by ER stress in Alzheimer's disease. J Chem Neuroanat. 28(1-2), 67–78. [PubMed: 15363492]

Kavalali ET (2015). The mechanisms and functions of spontaneous neurotransmitter release. Nat Rev Neurosci 16, 5–16. [PubMed: 25524119]

Kavalali ET (2019). Neuronal Ca(2+) signalling at rest and during spontaneous neurotransmission. J Physiol.

Klejman ME, Gruszczynska-Biegala J, Skibinska-Kijek A, Wisniewska MB, Misztal K, Blazejczyk M, Bojarski L, and Kuznicki J (2009). Expression of STIM1 in brain and puncta-like co-localization of STIM1 and ORAI1 upon depletion of Ca(2+) store in neurons. Neurochem Int 54, 49–55. [PubMed: 19013491]

Korkotian E, Oni-Biton E, and Segal M (2017). The role of the store-operated calcium entry channel Orai1 in cultured rat hippocampal synapse formation and plasticity. J Physiol 595, 125–140. [PubMed: 27393042]

Kushnireva L, Korkotian E, and Segal M (2021). Calcium Sensors STIM1 and STIM2 Regulate Different Calcium Functions in Cultured Hippocampal Neurons. Front. Synaptic Neurosci 12:573714. [PubMed: 33469426]

Li YC, Chanaday NL, Xu W, and Kavalali ET (2017). Synaptotagmin-1- and Synaptotagmin-7-Dependent Fusion Mechanisms Target Synaptic Vesicles to Kinetically Distinct Endocytic Pathways. Neuron, 93(3), 616–631.e3. [PubMed: 28111077]

Lim R, Oleskevich S, Few AP, Leao RN and Walmsley B (2003). Glycinergic mIPSCs in mouse and rat brainstem auditory nuclei: modulation by ruthenium red and the role of calcium stores. J Physiol 546.3, 691–699. [PubMed: 12562997]

Lin PY, Kavalali ET, and Monteggia LM (2018). Genetic Dissection of Presynaptic and Postsynaptic BDNF-TrkB Signaling in Synaptic Efficacy of CA3-CA1 Synapses. Cell reports, 24(6), 1550–1561. [PubMed: 30089265]

Liou J, Kim ML, Heo WD, Jones JT, Myers JW, Ferrell JE Jr., and Meyer T (2005). STIM is a Ca2+ sensor essential for Ca2+-store-depletion-triggered Ca2+ influx. Curr Biol 15, 1235–1241. [PubMed: 16005298]

Luarte A, Cornejo VH, Bertin F, Gallardo J, and Couve A (2018). The axonal endoplasmic reticulum: One organelle-many functions in development, maintenance, and plasticity. Dev Neurobiol 78, 181–208. [PubMed: 29134778]

Maciąg F, Majewski Ł, Boguszewski PM, Gupta RK, Wasilewska I, Wojtaś B, and Kuznicki J (2019). Behavioral and electrophysiological changes in female mice overexpressing ORAI1 in neurons. Biochimica et biophysica acta. Molecular cell research, 1866(7), 1137–1150. [PubMed: 30659848]

Mackay JP, Buren C, Smith-Dijak AI, Koch ET, Zhang P, Schmidt ME, Fung E, Nassrallah WB, Hayden MR, and Raymond LA (2020). Spontaneous Axonal ER Ca2+ Waves Mediate A Shift

From Action Potential-Dependent to Independent Glutamate Release in the YAC128 HD-Model. bioRxiv 2020.01.31.929299.

Majewski L, Maciąg F, Boguszewski PM, and Kuznicki J (2020). Transgenic Mice Overexpressing Human STIM2 and ORAI1 in Neurons Exhibit Changes in Behavior and Calcium Homeostasis but Show No Signs of Neurodegeneration. International journal of molecular sciences, 21(3), 842.

Maneshi MM, Toth AB, Ishii T, Hori K, Tsujikawa S, Shum AK, Shrestha N, Yamashita M, Miller RJ, Radulovic J, Swanson GT, and Prakriya M (2020). Orai1 Channels Are Essential for Amplification of Glutamate-Evoked Ca2+ Signals in Dendritic Spines to Regulate Working and Associative Memory. Cell reports, 33(9), 108464. [PubMed: 33264616]

Mitchell CB, Gasperini RJ, Small DH, and Foa L (2012). STIM1 is necessary for store-operated calcium entry in turning growth cones. J Neurochem 122, 1155–1166. [PubMed: 22712562]

Moccia F, Zuccolo E, Soda T, Tanzi F, Guerra G, Mapelli L, Lodola F, and D'Angelo E (2015). Stim and Orai proteins in neuronal Ca(2+) signaling and excitability. Front Cell Neurosci 9, 153. [PubMed: 25964739]

Mozhayeva MG, Sara Y, Liu X, and Kavalali ET (2002). Development of vesicle pools during maturation of hippocampal synapses. The Journal of neuroscience : the official journal of the Society for Neuroscience, 22(3), 654–665. [PubMed: 11826095]

Nosyreva E, and Kavalali ET (2010). Activity-dependent augmentation of spontaneous neurotransmission during endoplasmic reticulum stress. J Neurosci 30, 7358–7368. [PubMed: 20505103]

Oh-Hora M, Yamashita M, Hogan PG, Sharma S, Lamperti E, Chung W, Prakriya M, Feske S, and Rao A (2008). Dual functions for the endoplasmic reticulum calcium sensors STIM1 and STIM2 in T cell activation and tolerance. Nature immunology, 9(4), 432–443. [PubMed: 18327260]

Padamsey Z, Foster WJ, and Emptage NJ (2019). Intracellular Ca(2+) Release and Synaptic Plasticity: A Tale of Many Stores. The Neuroscientist : a review journal bringing neurobiology, neurology and psychiatry 25, 208–226.

Pavez M, Thompson AC, Arnott HJ, Mitchell CB, D'Atri I, Don EK, Chilton JK, Scott EK, Lin JY, Young KM, et al. (2019). STIM1 Is Required for Remodeling of the Endoplasmic Reticulum and Microtubule Cytoskeleton in Steering Growth Cones. The Journal of neuroscience : the official journal of the Society for Neuroscience 39, 5095–5114. [PubMed: 31023836]

Pchitskaya E, Kraskovskaya N, Chernyuk D, Popugaeva E, Zhang H, Vlasova O, and Bezprozvanny I (2017). Stim2-Eb3 Association and Morphology of Dendritic Spines in Hippocampal Neurons. Sci Rep 7, 17625. [PubMed: 29247211]

Pchitskaya E, Popugaeva E, and Bezprozvanny I (2018). Calcium signaling and molecular mechanisms underlying neurodegenerative diseases. Cell Calcium 70, 87–94. [PubMed: 28728834]

Perri ER, Thomas CJ, Parakh S, Spencer DM and Atkin JD (2016). The Unfolded Protein Response and the Role of Protein Disulfide Isomerase in Neurodegeneration. Front. Cell Dev.Biol 3:80. [PubMed: 26779479]

Pobre K, Poet GJ, and Hendershot LM (2019). The endoplasmic reticulum (ER) chaperone BiP is a master regulator of ER functions: Getting by with a little help from ERdj friends. The Journal of biological chemistry, 294(6), 2098–2108. [PubMed: 30563838]

Popugaeva E, Pchitskaya E, and Bezprozvanny I (2018). Dysregulation of Intracellular Calcium Signaling in Alzheimer's Disease. Antioxid Redox Signal 29, 1176–1188. [PubMed: 29890840]

Power JM and Sah P (2005). Intracellular calcium store filling by an L-type calcium current in the basolateral amygdala at subthreshold membrane potentials. J Physiol 562(Pt 2), 439–53. [PubMed: 15550460]

Pozzo-Miller LD, Pivovarova NB, Leapman RD, Buchanan RA, Reese TS and Andrews SB (1997). Activity-Dependent Calcium Sequestration in Dendrites of Hippocampal Neurons in Brain Slices. Journal of Neuroscience 17 (22), 8729–8738. [PubMed: 9348342]

Prakriya M, and Lewis RS (2015). Store-Operated Calcium Channels. Physiol Rev 95, 1383–1436. [PubMed: 26400989]

Putney JW (2009). Capacitative calcium entry: from concept to molecules. Immunol Rev 231, 10–22. [PubMed: 19754887]

Putney JW Jr. (1990). Capacitative calcium entry revisited. Cell Calcium 11, 611–624. [PubMed: 1965707]

Roos J, DiGregorio PJ, Yeromin AV, Ohlsen K, Lioudyno M, Zhang S, Safrina O, Kozak JA, Wagner SL, Cahalan MD, et al. (2005). STIM1, an essential and conserved component of store-operated Ca2+ channel function. J Cell Biol 169, 435–445. [PubMed: 15866891]

Ross WN (2012). Understanding calcium waves and sparks in central neurons. Nat Rev Neurosci 13, 157–168. [PubMed: 22314443]

Rusakov DA and Fine A (2003). Extracellular Ca2+ Depletion Contributes to Fast Activity-Dependent Modulation of Synaptic Transmission in the Brain. Neuron 37 (2), 287–297. [PubMed: 12546823]

Sano R, and Reed JC (2013). ER stress-induced cell death mechanisms. Biochim Biophys Acta 1833, 3460–3470. [PubMed: 23850759]

Schindelin J, Arganda-Carreras I, Frise E, Kaynig V, Longair M, Pietzsch T, Preibisch S, Rueden C, Saalfeld S, Schmid B, Tinevez JY, White DJ, Hartenstein V, Eliceiri K, Tomancak P, and Cardona A (2012). Fiji: an open-source platform for biological-image analysis. Nature methods, 9(7), 676–682. [PubMed: 22743772]

Shah SZA, Zhao D, Khan SH and Yang L (2015). Unfolded Protein Response Pathways in Neurodegenerative Diseases. J Mol Neurosci 57, 529–537. [PubMed: 26304853]

Shim S, Zheng JQ, and Ming GL (2013). A critical role for STIM1 in filopodial calcium entry and axon guidance. Mol Brain 6, 51. [PubMed: 24289807]

Simkus CRL and Stricker C (2002). The contribution of intracellular calcium stores to mEPSCs recorded in layer II neurones of rat barrel cortex. Journal of Physiology 545.2, 521–535.

Soboloff J, Rothberg BS, Madesh M, and Gill DL (2012). STIM proteins: dynamic calcium signal transducers. Nat Rev Mol Cell Biol 13, 549–565. [PubMed: 22914293]

Stewart SA, Dykxhoorn DM, Palliser D, Mizuno H, Yu EY, An DS, Sabatini DM, Chen IS, Hahn WC, Sharp PA, Weinberg RA, & Novina CD (2003). Lentivirus-delivered stable gene silencing by RNAi in primary cells. RNA (New York, N.Y.), 9(4), 493–501.

Sudhof TC (2013). Neurotransmitter release: the last millisecond in the life of a synaptic vesicle. Neuron 80, 675–690. [PubMed: 24183019]

Sugita S, Shin OH, Han W, Lao Y, and Südhof TC (2002). Synaptotagmins form a hierarchy of exocytotic Ca(2+) sensors with distinct Ca(2+) affinities. The EMBO journal, 21(3), 270–280. [PubMed: 11823420]

Sun S, Zhang H, Liu J, Popugaeva E, Xu NJ, Feske S, White CL 3rd, and Bezprozvanny I (2014). Reduced synaptic STIM2 expression and impaired store-operated calcium entry cause destabilization of mature spines in mutant presenilin mice. Neuron 82, 79–93. [PubMed: 24698269]

Voglmaier SM, Kam K, Yang H, Fortin DL, Hua Z, Nicoll RA, and Edwards RH (2006). Distinct endocytic pathways control the rate and extent of synaptic vesicle protein recycling. Neuron, 51(1), 71–84. [PubMed: 16815333]

Voleti R, Tomchick DR, Sudhof TC, and Rizo J (2017). Exceptionally tight membrane-binding may explain the key role of the synaptotagmin-7 C2A domain in asynchronous neurotransmitter release. Proc Natl Acad Sci U S A 114, E8518–E8527. [PubMed: 28923929]

Wegierski T, and Kuznicki J (2018). Neuronal calcium signaling via store-operated channels in health and disease. Cell Calcium 74, 102–111. [PubMed: 30015245]

Wei D, Mei Y, Xia J, and Hu H (2017). Orai1 and Orai3 Mediate Store-Operated Calcium Entry Contributing to Neuronal Excitability in Dorsal Root Ganglion Neurons. Frontiers in cellular neuroscience, 11, 400. [PubMed: 29311831]

Wen H, Hubbard JM, Rakela B, Linhoff MW, Mandel G and Brehm P (2013). Synchronous and asynchronous modes of synaptic transmission utilize different calcium sources. eLife art. no. e01206.

Wu Y, Whiteus C, Xu CS, Hayworth KJ, Weinberg RJ, Hess HF, and De Camilli P (2017). Contacts between the endoplasmic reticulum and other membranes in neurons. Proc Natl Acad Sci U S A 114, E4859–E4867. [PubMed: 28559323]

Xu J, Pang ZP, Shin OH, and Südhof TC (2009). Synaptotagmin-1 functions as a Ca2+ sensor for spontaneous release. Nature neuroscience, 12(6), 759–766. [PubMed: 19412166]

Xu W, Morishita W, Buckmaster PS, Pang ZP, Malenka RC, and Südhof TC (2012). Distinct neuronal coding schemes in memory revealed by selective erasure of fast synchronous synaptic transmission. Neuron, 73(5), 990–1001. [PubMed: 22405208]

Yap KAF, Shetty MS, Garcia-Alvarez G, Lu B, Alagappan D, Oh-Hora M, Sajikumar S and Fivaz M (2017). STIM2 regulates AMPA receptor trafficking and plasticity at hippocampal synapses. Neurobiology of learning and memory 138, 54–61. [PubMed: 27544849]

Zhang H, Wu L, Pchitskaya E, Zakharova O, Saito T, Saido T, and Bezprozvanny I (2015). Neuronal Store-Operated Calcium Entry and Mushroom Spine Loss in Amyloid Precursor Protein Knock-In Mouse Model of Alzheimer's Disease. J Neurosci 35, 13275–13286. [PubMed: 26424877]

Zhang I, and Hu H (2020). Store-Operated Calcium Channels in Physiological and Pathological States of the Nervous System. Frontiers in cellular neuroscience, 14, 600758. [PubMed: 33328896]

Highlights

- SOCE can potentiate excitatory spontaneous neurotransmission
- SOCE is mediated by STIM2 and drives neurotransmitter release through syt7
- Syt1 clamps SOCE-mediated spontaneous release
- SOCE/syt7 pathway participates in propagation of ER stress-related neuronal damage

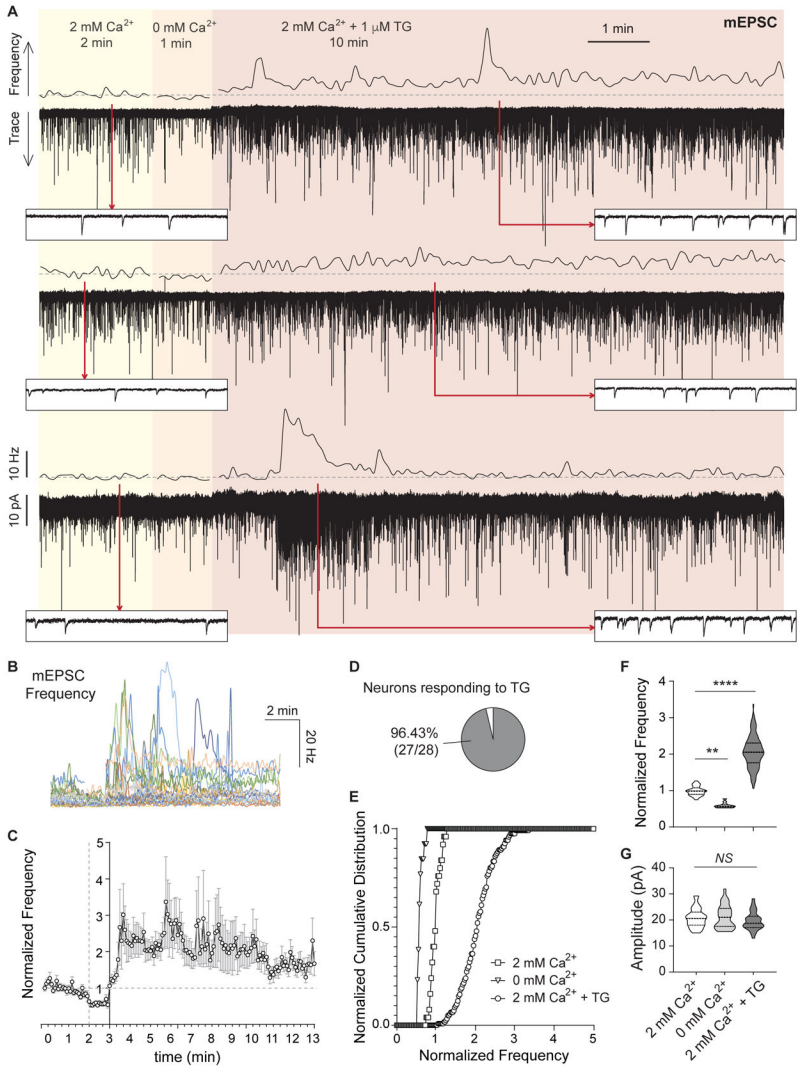

Figure 1. Ca^{2+} depletion from the ER augments spontaneous neurotransmission at excitatory synapses.

A. Three example traces (bottom of each pair) and 5 s moving averages of frequency (top of each pair) of mEPSC recorded from pyramidal hippocampal neurons. The same cell was continuously recorded while sequentially perfusing three different external solutions containing: 2 mM Ca^{2+} (2 min), 0 mM Ca^{2+} (1 min) and 2 mM Ca^{2+} with 1 μM TG (10 min). Dash line: average mEPSC frequency value of baseline (2 mM Ca^{2+}). Insets show a 1 s window at the time points marked by red arrows.

B. 5 s moving averages of mEPSC frequency for all the experiments performed.

C. Time course of average ± SEM of normalized to baseline mEPSC frequency.

D. Percentage of patched neurons showing a positive increase in mEPSC frequency upon TG perfusion. For each recording, a positive effect was defined as: ($Norm.freq_{TG}$-SD_{TG}) > ($Norm,\ freq_{baseline} + SD_{baseline}$)

E-F. Cumulative histogram and violin plots of normalized mEPSC frequency.

G. Violin plot of mEPSC amplitude.

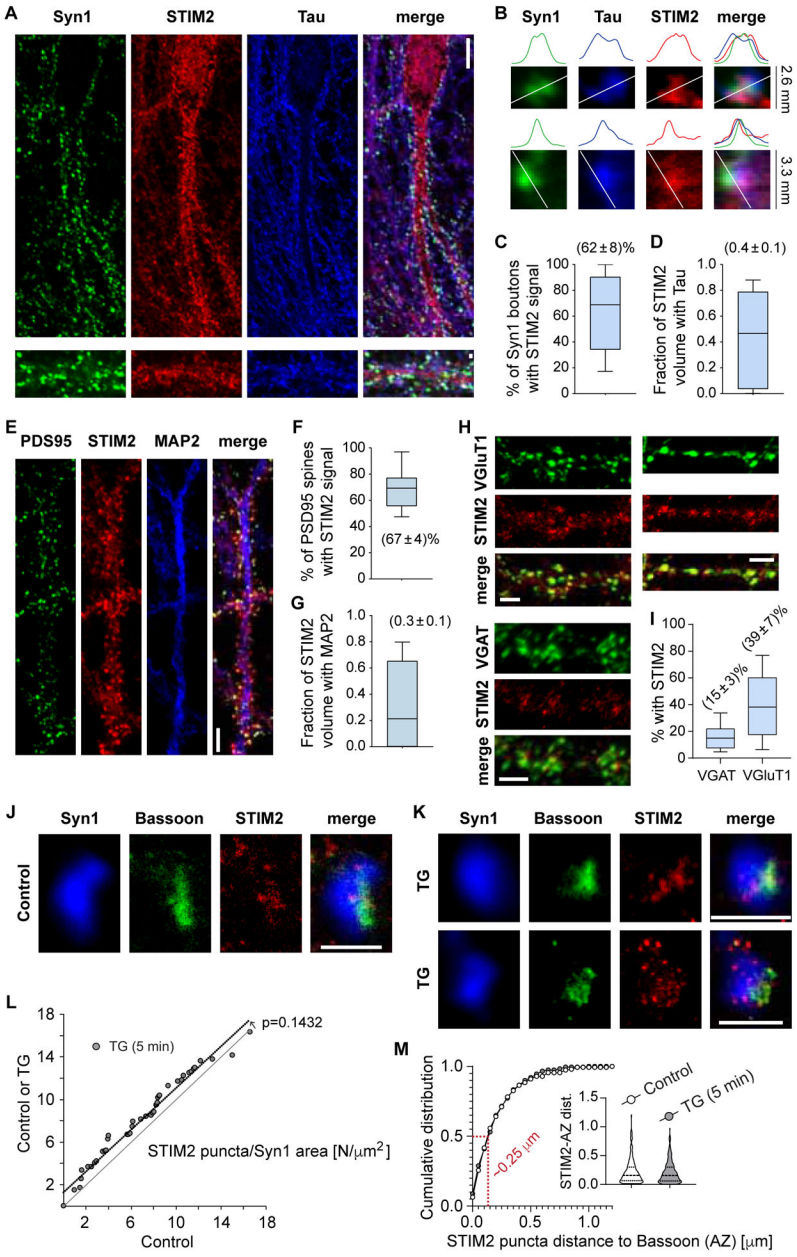

Figure 2. STIM2 is present at hippocampal presynaptic terminals.

A. Representative confocal images showing immunofluorescence staining of the presynaptic marker synapsin-1 (Syn1, green), the axonal marker Tau (blue) and STIM2 (red). White calibration bar for images in the right = 10 μm. White calibration bars for zoomed-in images of synapses on the left = 1 μm.

B. Detailed view of two example presynaptic boutons (top images) and line scans of intensity for each color (bottom). Observe the high degree of spatial co-localization of STIM2 with presynaptic markers.

C. 3D object-based co-localization analysis of syn1 positive boutons with STIM2 (count of number of syn1 objects containing STIM2 signal, expressed as percentage).

D. 3D volume analysis of STIM2 signal and the level of colocalization with Tau (to show the proportion of total neuronal STIM2 localized to axons).
For C and D: data obtained from 2 independent cultures, 2 coverslips, 13 images.
E. Representative confocal images showing immunofluorescence staining of the postsynaptic marker PSD95 (green), the dendrite marker MAP2 (blue) and STIM2 (red). White calibration bars = 5 μm.
F. 3D object-based co-localization analysis of PSD95 positive boutons with STIM2 (count of number of PSD95 objects containing STIM2 signal, expressed as percentage).
G. 3D volume analysis of STIM2 signal and the level of colocalization with MAP2 (to show the proportion of total neuronal STIM2 localized to dendrites).
For F and G: data obtained from 2 independent cultures, 2 coverslips, 13 images.
H. Representative confocal images showing immunofluorescence staining of STIM2 (red) and the glutamatergic or GABAergic markers VGluT1 (top, green) or VGAT (bootom, green), respectively. White calibration bars = 3 μm.
I. 3D object-based co-localization analysis of VGluT1 or VGAT positive boutons with STIM2 (count of number of VGluT1/VGAT objects containing STIM2 signal, expressed as percentage). Data from 2 coverslips, 14 images per group
J-K. 2-D STED images of individual synapses in control (unstimulated) and TG treated (1 μM, 5 min) conditions. Blue: synapsin-1 (confocal); green: Bassoon (STED); red: STIM2 (STED). White calibration bars = 1 μm.
L. Rank plot of number of STIM2 puncta per Syn1 area [$N/\mu m^2$] in control or TG versus control. P-value of the shift was obtained using ROC logistic analysis (3 coverslips per group, 2 cultures).
M. Cumulative histogram of distance to AZ of STIM2 puncta. Red: distance value at 50%. Inset: Violin plot.

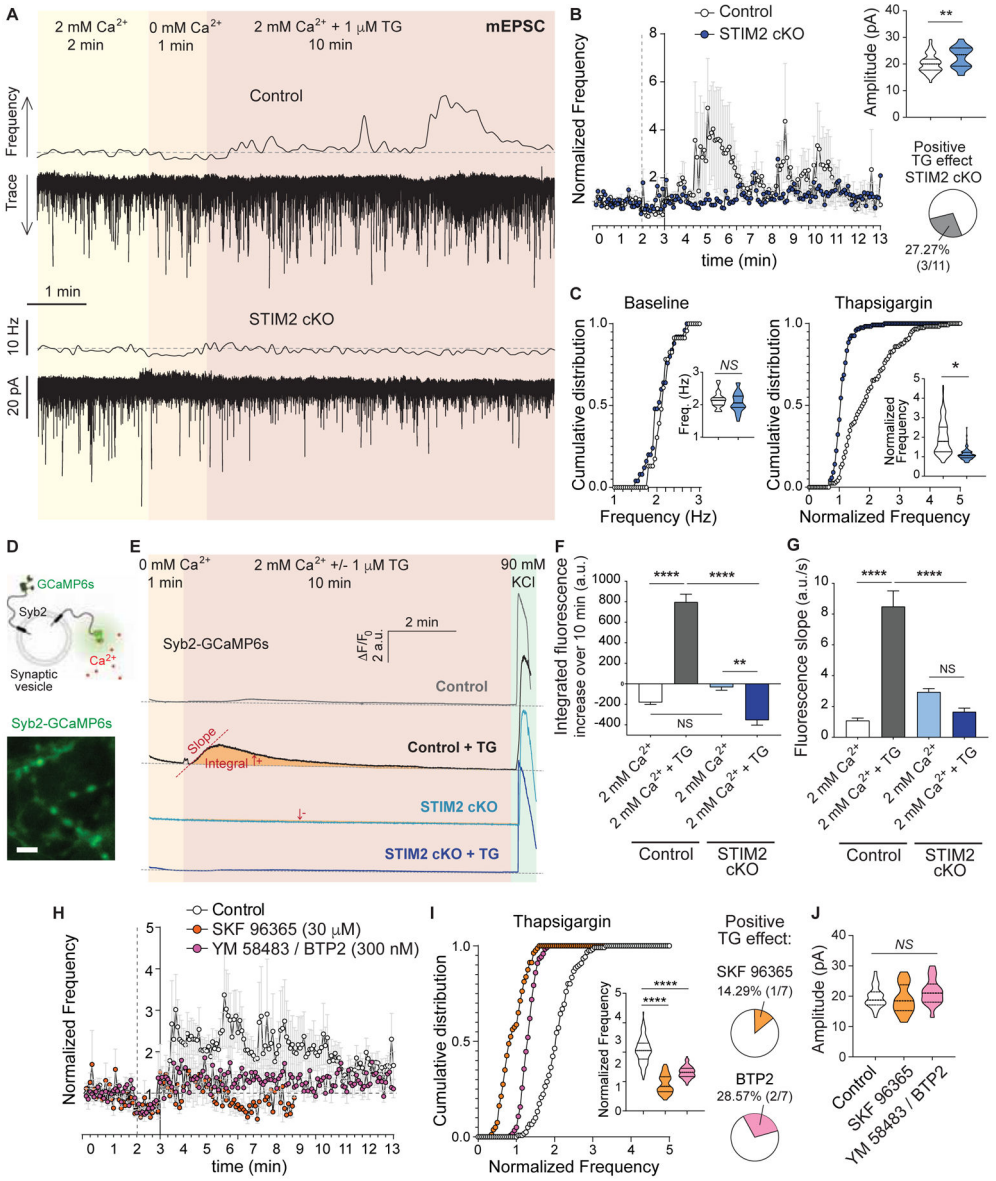

Figure 3. STIM2 and Orai are necessary for the ER Ca^{2+} depletion-mediated augmentation of excitatory spontaneous neurotransmission.

A. Example traces and 5 s moving averages of frequency of mEPSC recorded from wild type (control) and STIM2 cKO neurons (same experimental design as Figure 1A).

B. Time course of average ± SEM of mEPSC frequency normalized to baseline. Inset (top): Violin plot of mEPSC amplitude. Inset (bottom): Percentage of patched STIM2 cKO neurons showing a positive increase in mEPSC frequency upon TG perfusion.

C. Left: Cumulative histogram and violin plot (inset) of baseline mEPSC frequency. Right: Cumulative histogram and violin plot (inset) of mEPSC frequency during TG perfusion, normalized to baseline

D. Top: schematic representation of the presynaptic Ca^{2+} sensor syb2-GCaMP6s. Bottom: representative image of syb2-GCaMP6s showing presynaptic boutons stimulated with 90 mM KCl. White calibration bar = 5 μm.

E. Average syb2-GCaMP6s fluorescence traces for control (top, black-grey) and STIM2 cKO (bottom, blue) neurons. The same region was monitored for 1 min in extracellular solution containing 0 mM Ca^{2+} and then 2 mM Ca^{2+} with or without 1 μM TG was perfused. 90 mM KCl was perfused at the end of each experiment as a positive control.
F. Total area (integrated fluorescence) of the Ca^{2+} signal measured after perfusion of 2 mM Ca^{2+} with or without TG for each experimental group.
G. Initial rate of fluorescence increase (slope) after perfusion of 2 mM Ca^{2+} with or without TG for each experimental group.
H. Time course of average ± SEM of mEPSC frequency normalized to baseline in control neurons and treated with SKF 96365 (orange circles; 30 μM) or BTP2/YM 58483 (purple circles; 300 nM).
I. Left: Cumulative histogram and violin plot (inset) of mEPSC frequency during TG perfusion, normalized to baseline. Right: Percentage of patched neurons pretreated with the SOCE blockers that showed a positive increase in mEPSC frequency upon TG perfusion.
J. Violin plot of mEPSC amplitude.

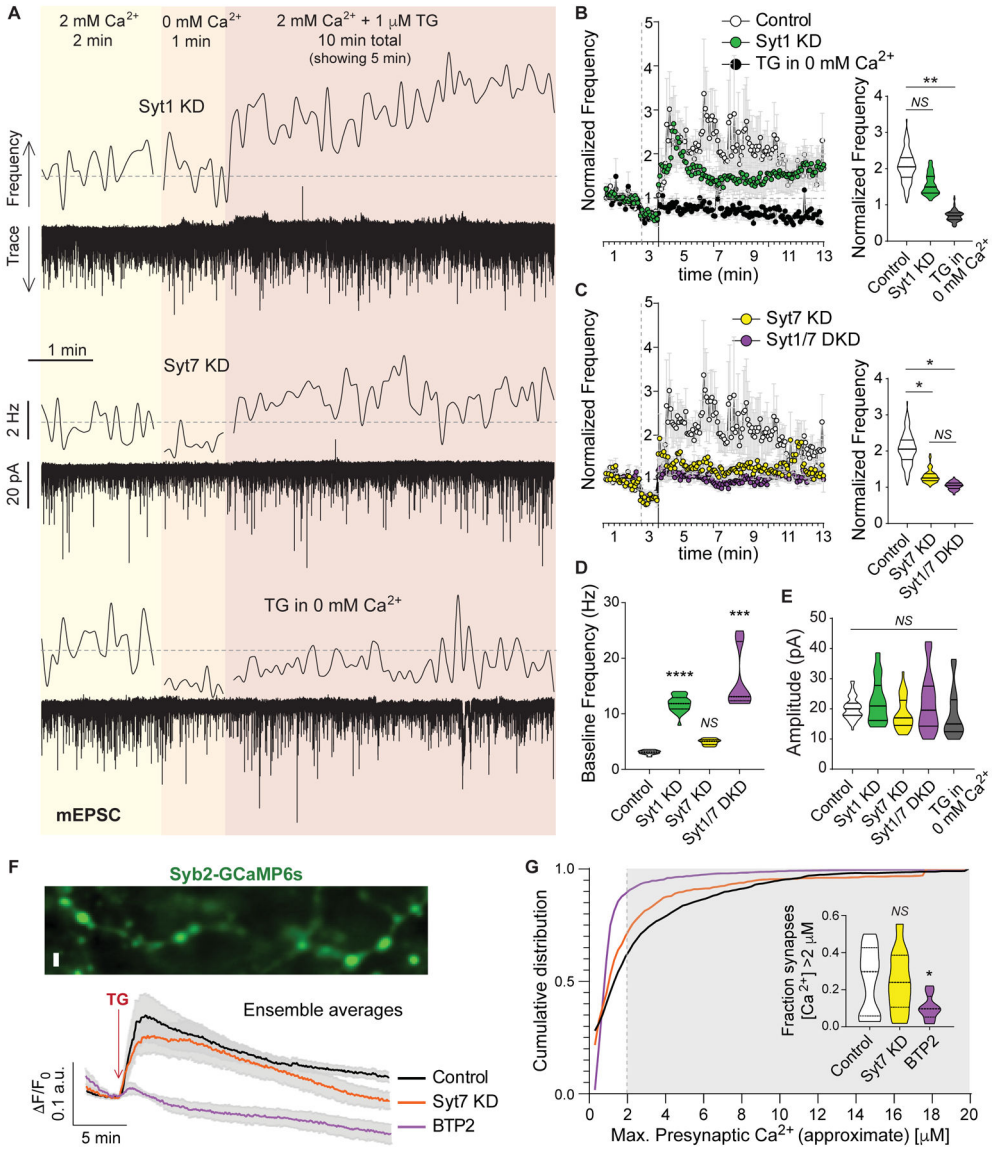

Figure 4. The Ca^{2+} sensor synaptotagmin-7 mediates the SOCE-dependent augmentation of spontaneous excitatory neurotransmission.

A. Example traces and 5 s moving averages of frequency of mEPSC recorded from syt1 KD (top) and syt7 KD (middle) neurons following the experimental design shown in Figure 1A. Using wild type (control) neurons, another set of experiments were performed perfusing TG in the absence (0 mM) of extracellular Ca^{2+} (bottom trace and average frequency).

B-C. Left: Time courses of average ± SEM mEPSC frequency normalized to baseline for control, syt1 KD, syt7 KD, syt1/7 DKD and TG in 0 mM Ca^{2+} experimental groups. Right: Violin plots of normalized mEPSC frequency.

D. Violin plot of baseline (2 mM Ca^{2+}) mEPSC frequency.

E. Violin plots of mEPSC amplitude for control, syt1 KD, syt7 KD, syt1/7 DKD and TG in 0 mM Ca^{2+} experimental groups.

F. Top: Representative image of syb2-GCaMP6s showing presynaptic boutons. White calibration bar = 2 μm. Bottom: Average syb2-GCaMP6s fluorescence traces for control (black line), syt7 KD (orange line) and BTP2 pretreated (purple line) neurons.
G. Cumulative histogram of maximal presynaptic Ca^{2+} signal reached after TG perfusion (i.e. peak amplitude converted to concentration, see Methods). Inset: Violin plot of Ca^{2+} concentration for synapses with increases above 2 μM after TG perfusion (corresponding to grey shaded area in histogram).

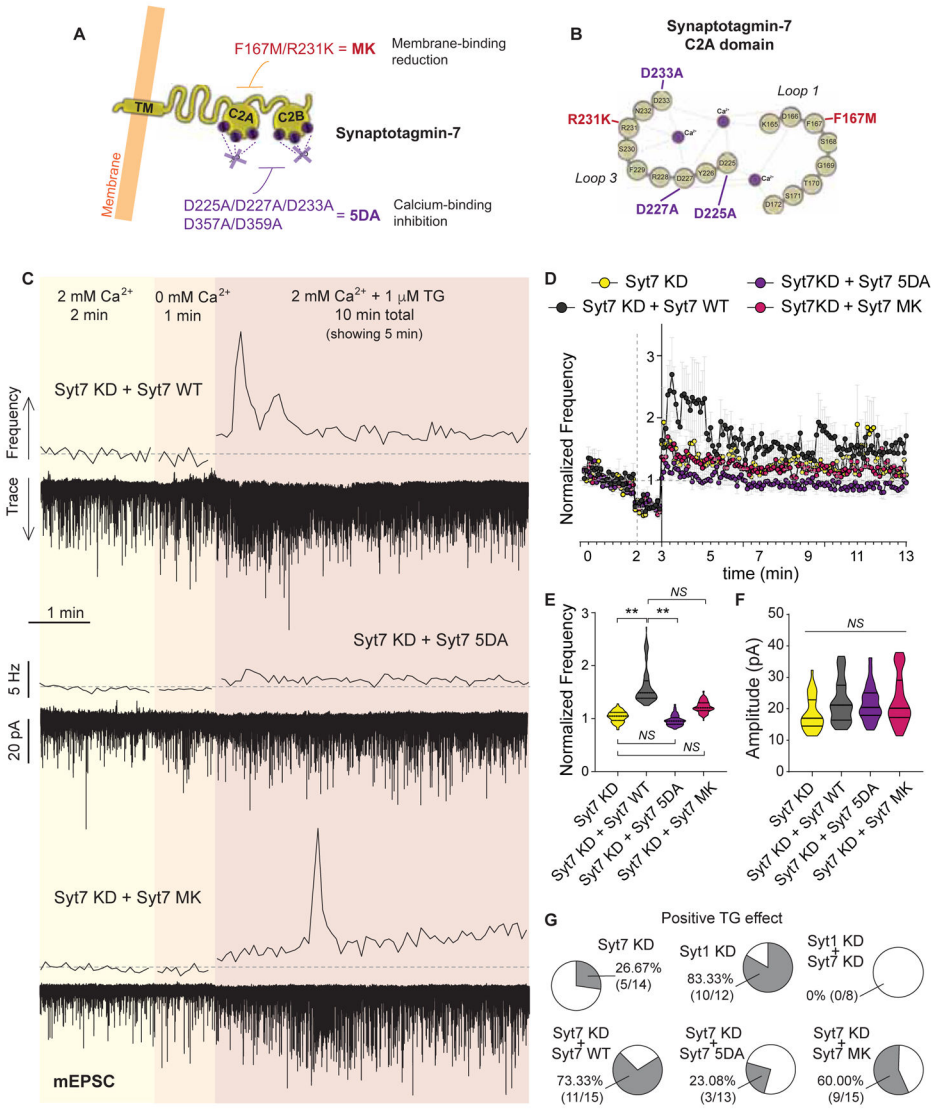

Figure 5. Ca^{2+} binding to synaptotagmin-7 mediates release of neurotransmitter after SOCE activation.

A. Schematic representation of syt7 structure and domains, showing the mutations performed in this work.

B. Detailed representation of the first Ca^{2+} binding domain (C2A) of syt7 and the mutation sites.

C. Example traces and 5 s moving averages of frequency of mEPSC recorded from syt7 KD neurons rescued with the full-length wild type (WT) syt7 protein (top), the 5DA mutant for of syt7 (middle) or the MK mutant (bottom); following the same experimental design as in Figure 1A.

D. Time course of average mEPSC frequency normalized to baseline, for syt7 KD and the rescue experiments with syt7 WT, syt7 5DA and syt7 MK.

E. Violin plot of normalized mEPSC frequency during TG perfusion.

F. Violin plot of mEPSC amplitude for syt7 KD neurons and syt7 KD with syt7 WT, syt7 5DA or syt7 MK.

G. Percentage of patched syt7 KD neurons and the rescue groups (WT, 5DA, MK) presenting an increase in mEPSC frequency upon TG perfusion.

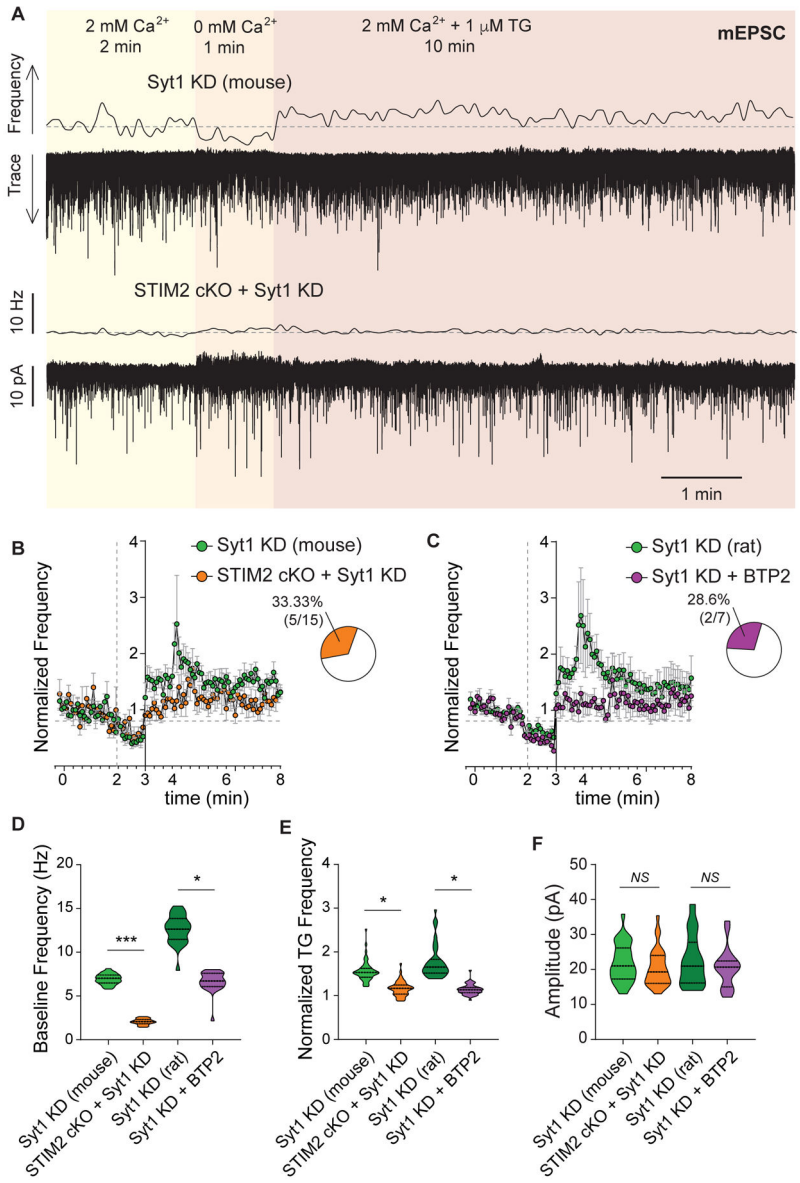

Figure 6. Synaptotagmin-1 clamps SOCE-driven spontaneous release.

A. Example traces and 5 s moving averages of frequency of mEPSC recorded from neurons deficient in syt1 (top) or depleted of both STIM2 and syt1 proteins (bottom; same experimental design as in Figure 1A).

B-C. Time courses of average mEPSC frequency normalized to baseline, for hippocampal dissociated neurons from mice (syt1 KD and syt1 KD + STIM2 cKO) from rats (syt1 KD and syt1 KD + BTP2). Insets: Percentage of patched neurons with a significant increase in mEPSC frequency upon TG perfusion (in syt1 KD plus either STIM2 cKO or BTP2).

D-F. Violin plots of baseline frequency (2 mM Ca^{2+}), normalized frequency during TG perfusion and amplitude of mEPSC for mouse (syt1 KD and syt1 KD + STIM2 cKO) and rat (syt1 KD and syt1 KD + BTP2) hippocampal neurons.

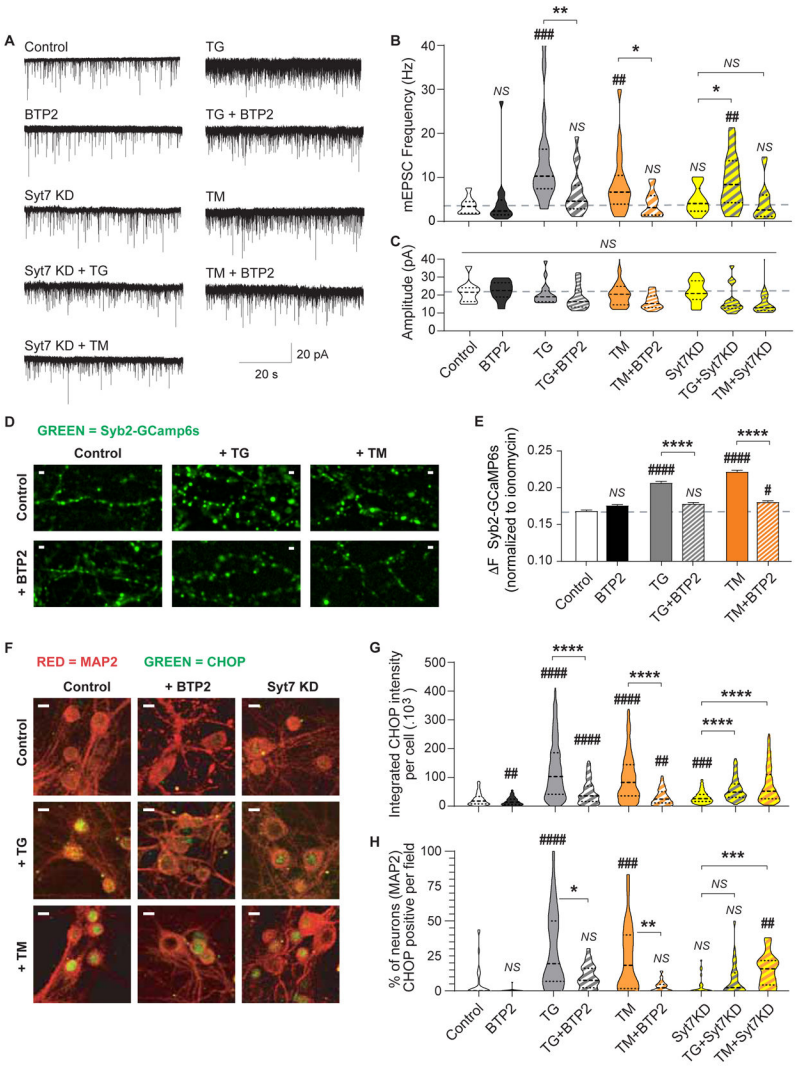

Figure 7. Upregulation of spontaneous neurotransmission and pro-apoptotic factors during chronic ER stress is mediated by SOCE and syt7.

A. Representative mEPSC recordings from each experimental group.

B-C. Violin plot of mEPSC frequency and amplitude for each experimental group. TG (300 nM), TM (5 μg/mL) and BTP2 (300 nM) were incubated in the culture media for 48h. Dashed line: average value of control group.

D. Representative fluorescence images of the presynaptic Ca^{2+} sensing probe, Syb2-GCaMP6s in control neurons and treated for 48 h with either TG or TM, in the presence or absence of BTP2. White calibration bar = 2 μm.

E. Syb2-GCaMP6s fluorescence intensity (ΔF) normalized to maximal ionomycin response for untreated (control) and 48 h treated groups (TM or TG with or without BTP2).

F. Representative images of neurons stained against MAP2 (red) and CHOP (green) for control (untreated) and neurons treated with TG or TM in combination with BTP2 or syt7 KD. White calibration bar = 10 μm.

G-H. Integrated fluorescence intensity per cell and number of CHOP positive neurons (presented as percentage) per image. Neuron segmentation was performed using the

binarized 3D MAP2 images, then the presence and intensity of CHOP fluorescence inside each 3D object (i.e. neuron) was quantified. Threshold to detect CHOP positive cells was defined using a negative control (cultures stained with secondary antibody only).

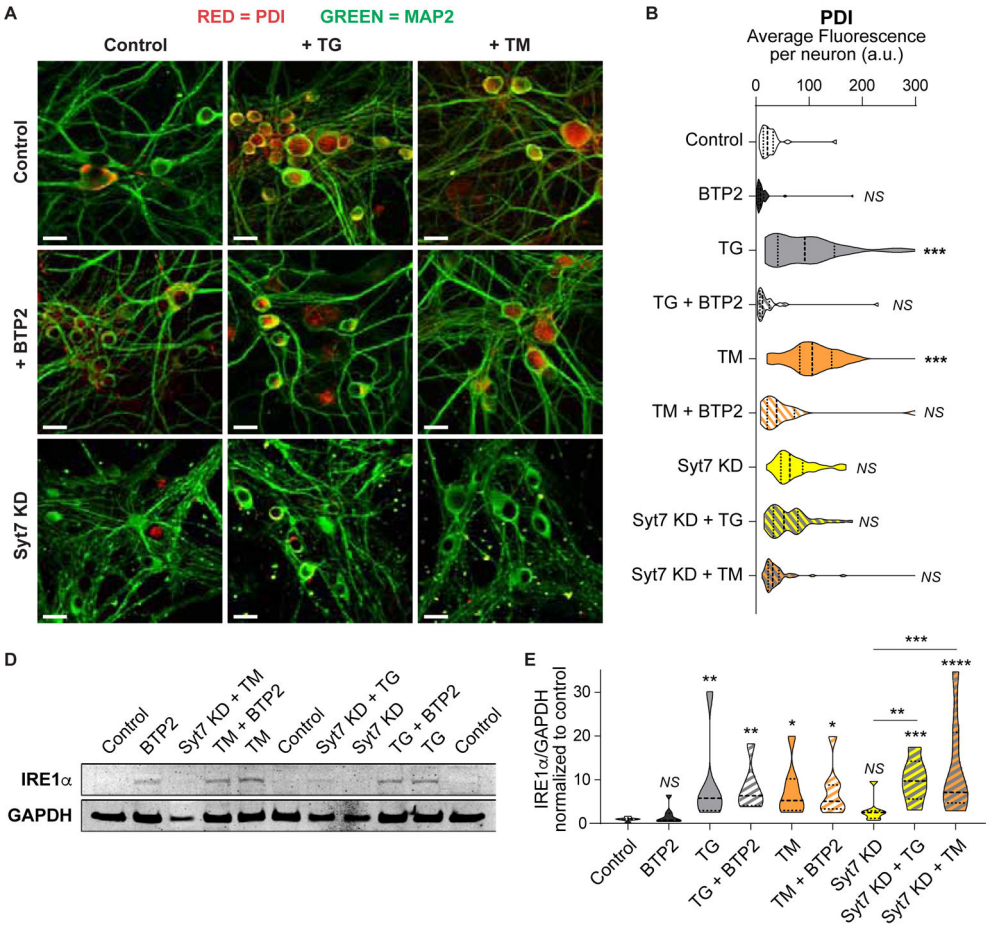

Figure 8. SOCE blockade or syt7 depletion can revert increased PDI levels but not BiP and IRE1α upregulation in chronic ER stress.

A. Representative confocal images of immunofluorescently labeled PDI (red) and MAP2 (green) in dissociated hippocampal neurons after 48 h incubation with TG or TM (with or without BTP2) to induce ER stress, in control or syt7 KD neurons. White scale bars = 20 μm.

B. Average PDI fluorescence per neuron in control, syt7 KD, TG and TM, with or without BTP2, treated groups. 3D images of MAP2 were binarized and segmented, then PDI fluorescence was measured inside each MAP2-positive object (i.e. neurons).

C. Example Western blot image from one representative experiment. Top: IRE1μ (130 KDa). Bottom: GAPDH (loading control). ER stress was induced by incubation with TG or TM for 48 h in control, BTP2 treated or syt7 KD dissociated hippocampal neurons.

D. Quantification of IRE1μ levels (normalized to GAPDH and relativized to control).

KEY RESOURCES TABLE

REAGENT or RESOURCE	SOURCE	IDENTIFIER
Antibodies		
Guinea pig polyclonal anti-Tau	Synaptic Systems	Cat# 314 004, RRID:AB_1547385
Guinea pig polyclonal anti-MAP2	Synaptic Systems	Cat# 188 004, RRID:AB_2138181
Mouse monoclonal anti-Synapsin 1	Synaptic Systems	Cat# 106 011, RRID:AB_2619772
Rabbit polyclonal anti-Synapsin1	Synaptic Systems	Cat# 106 103, RRID:AB_11042000
Mouse monoclonal anti-PSD95	Synaptic Systems	Cat# 124 011, RRID:AB_10804286
Mouse monoclonal anti-Rab-GDI1	Synaptic Systems	Cat# 130 011, RRID:AB_1966443
Rabbit monoclonal anti-GAPDH	Cell Signaling	Cat# 2118, RRID:AB_561053
Rabbit polyclonal anti-Synaptotagmin 7	Synaptic Systems	Cat# 105 173, RRID:AB_887838
Mouse monoclonal anti-Synaptotagmin 1	Synaptic Systems	Cat# 105 011, RRID:AB_887832
Mouse monoclonal anti-CHOP (L63F7)	Cell Signaling	Cat# 2895, RRID:AB_2089254
Rabbit polyclonal anti-STIM2	Cell Signaling	Cat# 4917, RRID:AB_2198021
Rabbit monoclonal anti-STIM1 (D88E10)	Cell Signaling	Cat# 5668, RRID:AB_10828699
anti IRE1α (14C10) - Rabbit monoclonal	Cell Signaling	Cat# 3294, RRID:AB_823545
anti PDI (C81H6) - Rabbit monoclonal	Cell Signaling	Cat# 3501, RRID:AB_2156433
anti GRP78 BiP - Rabbit polyclonal	Abcam	Cat# ab21685, RRID:AB_2119834
anti Basoon - Guinea pig polyclonal	Synaptic Systems	Cat# 141 004, RRID:AB_2290619
anti VGLUT1 - guinea pig antiserum	Synaptic Systems	Cat# 135 304, RRID:AB_887878
anti VGAT - guinea pig antiserum	Synaptic Systems	Cat# 131 004, RRID:AB_887873
Chemicals, Peptides, and Recombinant Proteins		
Tunicamycin from Streptomyces sp.	Sigma-Aldrich	Catalog # T7765-1MG
Thapsigargin	Sigma-Aldrich	Catalog # T9033-5MG
BTP2	Sigma-Aldrich	Catalog # 203890-5MG
SKF 96365	Tocris	Catalog # 1147
D(−)-2-Amino-5-phosphonopentanoic acid (AP-5)	Sigma-Aldrich	Catalog # A8054
Tetrodotoxin (TTX)	Enzo Life Sciences	Catalog # BML-NA120-0001
Picrotoxin (PTX)	Sigma-Aldrich	Catalog # P1675
6-cyano-7-nitroquinoxaline-2,3-dione (CNQX)	Sigma-Aldrich	Catalog # C239-100MG
Trypsin from bovine pancreas	Sigma-Aldrich	Catalog # T9935
DNase	Sigma-Aldrich	Catalog # D5025-375KU
Matrigel	Corning	Catalog # 354234
FuGENE 6	Promega	Catalog # E2692
QX-314	EMD-Millipore	Catalog # 552233
LIVE/DEAD Viability/Cytotoxicity Kit for mammalian cells	Thermofisher / Molecular Probes	Catalog # L3224
Ionomycin, free acid	Tocris	Catalog # 1234
A23187, free acid	Tocris	Catalog # 2092
Experimental Models: Cell Lines		

REAGENT or RESOURCE	SOURCE	IDENTIFIER
Highly transfectable derivative of human embryonic kidney-293 epithelial adherent cells (HEK293T)	ATCC	Catalog # CRL-1573
Experimental Models: Organisms/Strains		
STIM2 fl/fl C57BL/6 mice pups (P0-1)	Oh-Hora et al., 2008	N/A
Sprague-Dawley rat pups (P2-P4)	Charles River	N/A
Recombinant DNA		
Plasmid: pCMV-VSV-G (lentiviral packaging)	Adgene; Stewart et al., 2003	Catalog # 8454
Plasmid: pRSV-REV (lentiviral packaging)	Adgene; Dull et al., 1998	Catalog # 12253
Plasmid: pMDLg/pRRE (lentiviral packaging)	Adgene; Dull et al., 1998	Catalog # 12251
Plasmid: pFUGW-VGluT1-pHGFP	Voglmaier et al., 2006	N/A
Plasmid: pFUGW-Synaptobrevin2-GCaMP6s	Li et al., 2017	N/A
Plasmid: FCK(1.3)GW-ER-GCAM P6-150	AddGene; de Juan-Sanz et al., 2017	Plasmid #86918
Plasmid: L309-mCherry-Syt1 KD shRNA	Xu et al., 2012, Bacaj et al., 2013	N/A
Plasmid: L307-Syt7 KD shRNA	Bacaj et al., 2013	N/A
Plasmid: pFUGW-Syt7 WT (shRNA resistant)	Li et al., 2017	N/A
Plasmid: pFUGW-Syt7 5DA (shRNA resistant)	Bacaj et al., 2015	N/A
Plasmid: pFUGW-Syt7 MK	Voleti et al., 2017	N/A
Plasmid: pFUGW-GFP-Cre	Sequence from Lin et al., 2018	N/A
Plasmid: human STIM1 in pDS_XB-YFP vector	Brandman et al., 2007	N/A
Plasmid: human STIM2 in pDS_XB-YFP vector	Brandman et al., 2007	N/A
Rat STIM1 shRNA 1	GCATGGAAGGCATCAGAAGTGTATAACTG	
Rat STIM1 shRNA 2	GTCCCTGGATGACGTGGATCATAAAATCT	
Rat STIM2 shRNA 1	GGCTGAAAAGGAGTTTGAACTGAGAAGCA	
Rat STIM2 shRNA 2	GCCAGAAGCAGTAGTTTATGCCGCTCTCG	
Scramble shRNA control	GCACTACCAGAGCTAACTCAGATAGTACT	
Software and Algorithms		
Matlab script for pHluorin analysis	Chanaday et al., 2018a	N/A
Fiji	Schindelin et al., 2012	N/A
GelAnalyzer 2010a	http://www.gelanalyzer.com/	N/A